Multidecadal trend analysis of aerosol radiative properties at a global scale

Martine Collaud Coen[1], Elisabeth Andrews[2,3], Andrés Alastuey[4], Todor Petkov Arsov[5], John Backman[6], Benjamin T. Brem[7], Nicolas Bukowiecki[8], Cédric Couret[9], Konstantinos Eleftheriadis[10], Harald Flentje[11], Markus Fiebig[12], Martin Gysel-Beer[7], Jenny L. Hand[13], András Hoffer[14], Rakesh Hooda[4,15], Christoph Hueglin[16], Warren Joubert[17], Melita Keywood[18], Jeong Eun Kim[19], Sang-Woo Kim[20], Casper Labuschagne[17], Neng-Huei Lin[21], Yong Lin[12], Cathrine Lund Myhre[12], Krista Luoma[22], Hassan Lyamani[23,24], Angela Marinoni[25], Olga L. Mayol-Bracero[26], Nikos Mihalopoulos[27], Marco Pandolfi[4], Natalia Prats[28], Anthony J. Prenni[29], Jean-Philippe Putaud[30], Ludwig Ries[9], Fabienne Reisen[18], Karine Sellegri[31], Sangeeta Sharma[32], Patrick Sheridan[3], James Patrick Sherman[33], Junying Sun[34], Gloria Titos[23,24], Elvis Torres[26], Thomas Tuch[35], Rolf Weller[36], Alfred Wiedensohler[35], Paul Zieger[37,38], Paolo Laj [39,40,41]

[1] Federal Office of Meteorology and Climatology, MeteoSwiss, Payerne, Switzerland
[2] Cooperative Institute for Research in Environmental Sciences, University of Colorado, Boulder, CO, USA
[3] NOAA/Earth Systems Research Laboratory Boulder, CO, USA
[4] Institute of Environmental Assessment and Water Research (IDAEA), Spanish Research Council (CSIC), Barcelona, Spain
[5] Institute for Nuclear Research and Nuclear Energy, Bulgarian Academy of Sciences, Sofia, Bulgaria
[6] Atmospheric composition research, Finnish Meteorological Institute, Helsinki, Finland
[7] Laboratory of Atmospheric Chemistry, Paul Scherrer Institute, Villigen PSI, Switzerland
[8] Atmospheric Sciences, Department of Environmental Sciences, University of Basel, Basel, Switzerland
[9] German Environment Agency (UBA), Zugspitze, Germany.
[10] Institute of Nuclear and Radiological Science & Technology, Energy & Safety N.C.S.R. "Demokritos", Attiki, Greece
[11] German Weather Service, Meteorological Observatory Hohenpeissenberg, Hohenpeißenberg, Germany
[12] NILU – Norwegian Institute for Air Research, Kjeller, Norway
[13] Cooperative Institute for Research in the Atmosphere (CIRA), Colorado State University, Fort Collins, CO, USA
[14] MTA-PE Air Chemistry Research Group, Veszprém, Hungary
[15] The Energy and Resources Institute, IHC, Lodhi Road, New Delhi, India
[16] Empa, Swiss Federal Laboratories for Materials Science and Technology, Duebendorf, Switzerland
[17] South African Weather Service, Research Department, Stellenbosch, South Africa
[18] CSIRO Oceans and Atmosphere, PMB1 Aspendale VIC, Australia
[19] Environmental Meteorology Research Division, National Institute of Meteorological Sciences, Seogwipo, Korea
[20] School of Earth and Environmental Sciences, Seoul National University, Seoul, Korea
[21] Department of Atmospheric Sciences, National Central University, Taoyuan, Taiwan
[22] Institute for Atmospheric and Earth System Research, University of Helsinki, Helsinki, Finland
[23] Andalusian Institute for Earth System Research, IISTA-CEAMA, University of Granada, Junta de Andalucía, Granada, Spain
[24] Department of Applied Physics, University of Granada, Granada, Spain
[25] Institute of Atmospheric Sciences and Climate, National Research Council of Italy, Bologna, Italy
[26] University of Puerto Rico, Rio Piedras Campus, San Juan, Puerto Rico
[27] Environmental Chemistry Processes Laboratory, Department of Chemistry, University of Crete, Heraklion, Greece.
[28] Izaña Atmospheric Research Center, State Meteorological Agency (AEMET), Tenerife, Spain
[29] National Park Service, Air Resources Division, Lakewood, CO, USA
[30] European Commission, Joint Research Centre (JRC), Ispra, Italy

[31] Université Clermont Auvergne, CNRS, Laboratoire de Météorologie Physique (LaMP), Clermont-Ferrand, France
[32] Climate Chemistry Measurements Research, Climate Research Division, Environment and Climate Change Canada, Toronto, Canada
[33] Department of Physics and Astronomy, Appalachian State University, Boone, NC USA
[34] State Key Laboratory of Severe Weather & Key Laboratory of Atmospheric Chemistry of CMA, Chinese Academy of Meteorological Sciences, Beijing, China
[35] Leibniz Institute for Tropospheric Research (TROPOS), Leipzig, Germany
[36] Glaciology Department, Alfred-Wegener-Institut Helmholtz Zentrum für Polar- und Meeresforschung, Bremerhaven, Germany
[37] Department of Environmental Science and Analytical Chemistry, Stockholm University, Stockholm, Sweden
[38] Bolin Centre for Climate Research, Stockholm University, Stockholm, Sweden
[39] Univ. Grenoble Alpes, CNRS, IRD, Grenoble-INP, IGE, 38000 Grenoble, France
[40] CNR-ISAC, National Research Council of Italy – Institute of Atmospheric Sciences and Climate, Bologna, Italy
[41] University of Helsinki, Atmospheric Science division, Helsinki, Finland

Correspondence: Martine Collaud Coen (martine.collaudcoen@meteoswiss.ch)

Abstract

In order to assess the global evolution of aerosol parameters affecting climate change, a long-term trend analyses of aerosol optical properties were performed on time series from 52 stations situated across five continents. The time series of measured scattering, backscattering and absorption coefficients as well as the derived single scattering albedo, backscattering fraction, scattering and absorption Ångström exponents covered at least 10 years and up to 40 years for some stations. The non-parametric seasonal Mann-Kendall (MK) statistical test associated with several prewhitening methods and with the Sen's slope were used as main trend analysis methods. Comparisons with General Least Mean Square associated with Autoregressive Bootstrap (GLS/ARB) and with standard Least Mean Square analysis (LMS) enabled confirmation of the detected MK statistically significant trends and the assessment of advantages and limitations of each method. Currently, scattering and backscattering coefficients trends are mostly decreasing in Europe and North America and are not statistically significant in Asia, while polar stations exhibit a mix of increasing and decreasing trends. A few increasing trends are also found at some stations in North America and Australia. Absorption coefficients time series also exhibit primarily decreasing trends. For single scattering albedo, 52% of the sites exhibit statistically significant positive trends, mostly in Asia, Eastern/Northern Europe and Arctic, 18% of sites exhibit statistically significant negative trends, mostly in central Europe and central North America, while the remaining 30% of sites have trends, which are not statistically significant. In addition to evaluating trends for the overall time series, the evolution of the trends in sequential 10 year segments was also analyzed. For scattering and backscattering, statistically significant increasing 10 year trends are primarily found for earlier periods (10 year trends ending in 2010-2015) for polar stations and Mauna Loa. For most of the stations, the present-day statistically significant decreasing 10 year trends of the single scattering albedo were preceded by not statistically significant and statistically significant increasing 10 year trends. The effect of air pollution abatement policies in continental North America is very obvious in the 10 year trends of the scattering coefficient – there is a shift to statistically significant negative trends in 2010-2011 for all stations in the eastern and central US. This long-term trend analysis of aerosol radiative properties with a broad spatial coverage enables a better global view of potential aerosol effects on climate changes.

1. Introduction

Climate change has been considered as a premier global problem in the scientific community for decades. Thirty years ago, the community organized to produce the first Intergovernmental Panel on Climate Change (IPCC) report (IPCC, 1990) about the state of scientific, technical and socio-economic knowledge on climate change, its impacts and future risks, and options for reducing the rate at which climate change was taking place. Aerosols have been recognized as an important active climate forcing agent since the 1970's and, in the last IPCC report (IPCC, 2013), the impact of aerosols on the atmosphere was still considered as one of the most significant and uncertain aspects of climate change projections and, for the first time, global decadal trend analysis of aerosol optical properties was reported. The magnitude of aerosol forcing was assessed to be – 0.45 (–0.95 to +0.05) Wm^{-2} for aerosol alone and –0.9 (–1.9 to –0.1) Wm^{-2} when aerosol/cloud feedbacks were accounted for.

Aerosol optical properties are the relevant parameters that determine the radiative forcing of particulate matter. While some of these optical properties are currently measured by satellite (Choi et al., 2019), airborne and ground-based remote sensing technologies (https://aeronet.gsfc.nasa.gov/, www.earlinet.org), the ground-based, in-situ measurements represent some of the longest time series, allowing assessment of the long-term time evolution of aerosol radiative properties in the lower troposphere.

The first in-situ measurement network began in the mid 1970's at several remote locations (Bodhaine et al., 1995). Through national, international programs and/or on individual organisation's initiatives, the number of stations with systematic aerosol monitoring activities in regional background locations has continued to increase since the 1990's. As of 2017 absorption has been measured for at least 1 year (y) at 50 sites, for 5 y at 37 sites and for 10 y at 20 sites, while scattering has been measured for at least 1 y at 56 sites, for 5 y at 45 sites and for 10 y at 30 sites. The companion paper (Laj et al., submitted) provides a historical view and a complete description of the present networks for aerosol measurements. The longest datasets cover up to 40 y of measurements (BRW (40 y), SPO (40 y), and MLO (31 y) (see Table 1 for station's acronyms), whereas some stations with long time series recently closed or moved (THD, SGP, MUK, CPT). The spatial and temporal variability of aerosol properties is extremely high due to the short lifetime of aerosol particles (on the order of days to weeks), the wide variety of sources, as well as the chemical and microphysical processing occurring in the atmosphere; a dense network of stations is consequently required to obtain a global view of aerosol changes. The growing number of stations with long-term (>10 y) time series of aerosol particles optical properties - 24 in 2010 (Collaud Coen et al., 2013, hereafter referred to as CC2013) and now 52 in 2016-2018 - is a positive factor. Detracting from that growth is the continued lack of sites in South America, Africa, Oceania and Asia.

Long-term measurements are the only possible approach for detecting change in atmospheric composition resulting from either changes in natural or anthropogenic emissions and/or changes in atmospheric processes and sinks. However, detecting long-term trends of aerosol optical properties remains a challenge, due to their high natural variability, uncertainties caused by changes and biases in measurement methodology, the ill-defined statistical distribution of the parameters, the presence of high autocorrelation in aerosol parameters, as well as the occasional issues regarding traceability of historic operating procedures. Trend analysis can only be performed on time series without break points or on homogenized time series that account for changes in measurement conditions (e.g. relocations, instrument calibration/repair/upgrades, inlet changes) (CC2013). Once homogenized data sets are available, appropriate techniques must be used to identify potential trends. The trend analysis methodology must take into account the non-normal distribution of most aerosol parameters, the high autocorrelation of the parameters, and the presence of gaps and negatives in the datasets.

In this current analysis, a considerable effort was made to detect time series break points, to find explanations for them in the logbooks and station history and, if possible, to correct or homogenize the time series. These homogenized time series were then subjected to an array of statistical tests to identify trends. These tests include: (1) the non-parametric Mann-Kendall test (thereafter

referred to as the MK test) associated with the Sen's slope. The applied MK test is however applied with a new pre-whitening method (Collaud Coen et al., in preparation), (2) a Generalised Least Squares (GLS) method associated with a Monte-Carlo bootstrap algorithm and (3) the Least-Mean Squares fit (LMS). While the MK test with pre-whitening was considered the most robust method, the other tests were included to allow a comparison between various simple and frequently used methods.

The first global long-term trend analyses of aerosol optical properties, number concentration and particle size distribution (CC2013 and Asmi et al., 2013) covered 2001-2010 as the shortest period as well as longer periods if data were available. The main observations were: (1) a general statistically significant (ss) -at 95% confidence level- decrease of number concentration, scattering and absorption coefficients in North America, (2) a ss decrease of number concentration in northeastern Europe, (3) no ss trend in central Europe for all the parameters and (4) no ss scattering coefficient trends but increasing 10 y absorption coefficient and number concentration trends in polar regions. These trends were related to the decrease in anthropogenic primary aerosol emissions and in precursors of secondary aerosol formation. The high altitude station Mauna Loa (MLO) in the Pacific was unique in exhibiting increasing optical properties trends that were mostly attributed to long-range transport from Asia. The results in CC2013 are in line with the 1996-2013 trend analysis at the BND and SGP stations in North America (Sherman et al., 2015) showing decreasing scattering coefficient and sub-micron scattering fraction and increasing backscattering fraction. More recently, Pandolfi et al. (2018) presented the long-term trends of in-situ surface aerosol particle optical properties (scattering) measured in Europe until 2015. The ss decreasing trends of aerosol particle scattering observed in Europe at around 40% of the stations (mostly in Nordic and Baltic countries and southwestern Europe) was attributed to the implementation of continental to local emission mitigation strategies. Pandolfi et al. (2018) also reported that the scattering Ångström exponent decreased at around 20% for the European stations included in their study (at remote Nordic and Baltic locations and at two mountain sites in central and eastern Europe), whereas an increase was observed at 15% of the stations (one urban site in southwestern Europe and one in central Europe). In the same study, the backscattering fraction was observed to increase. Trends in horizontal visibility synoptic observations over 1929-2013 from 4000 stations over the US, Europe and Asia (Li et al., 2016) generally agreed with extinction coefficient trends with a significant decrease in all regions but with different evolutions of the trends. Hand et al. (2014) also found a significant drop of the ambient light extinction coefficient at all IMPROVE (Interagency Monitoring of Protected Visual Environment, http://vista.cira.colostate.edu/Improve/) stations over the 1990s through 2011 with a larger decrease in the eastern US. To our knowledge, no further trend analyses of surface in-situ aerosol optical properties involving a network of stations or several stations have been published up to now.

This study is part of the SARGAN (in-Situ AeRosol GAW observing Network) initiative (see companion paper Laj et al. (submitted)) with the objective of supporting a global aerosol monitoring network to become a GCOS (Global Climate Observing System) associated network. This trend analysis is intended to answer the following questions:

1) Are there homogeneous global long-term trends in aerosol optical properties? Do they differ as a function of the length of the data series? How do the trends evolve with time?

2) Are there regional similarities or differences in the observed trends among stations? Are there similarities or differences in trends among aerosol parameters at a regional and global scale?

3) How do the observed optical property trends compare with trends in other aerosol and gaseous properties reported in the literature?

The results of this study provide the best representation of change in surface aerosol optical properties considering the available in-situ aerosol optical properties datasets and highlight the possible side effects of air pollution control policies on radiative forcing.

2. Experimental

2.1 Measurement sites

The long-term trend analysis presented in this study analyzes in-situ aerosol time series from 52 observatories worldwide shown in Fig. 1 with site information listed in Table 1. The global network,
5   which is a subset of the station network described in Laj et al. (submitted), comprises 16 stations in Europe, 21 stations in North America, 5 in Asia, 2 sites in Africa, 6 sites in the polar regions and 2 in the southwest Pacific. The stations included in this study are primarily located in rural or remote areas and are expected to exhibit regional to large scale representativeness (e.g., Wang et al., 2018). Apart from MUK, all the stations are regional or global GAW (Global Atmospheric
10 Watch, https://gawsis.meteoswiss.ch/GAWSIS//index.html#/) sites or IMPROVE stations. The GAW aerosol data are archived at and available from the World Data Centre for Aerosol (WDCA, http://www.gaw-wdca.org) located at the Norwegian Institute for Air Research (NILU). The WDCA data repository is the database EBAS (http://ebas.nilu.no), an e-infrastructure shared with other frameworks targeting atmospheric aerosol properties, such as the Co-operative Programme for
15 Monitoring and Evaluation of the Long-range Transmission of Air pollutants in Europe (EMEP) and the European Aerosols, Clouds, and Trace gases Research InfraStructure Network (ACTRIS). The IMPROVE data are available from the IMPROVE website (http://vista.cira.colostate.edu/improve/Data/data.htm), and from the WDCA. To ensure the long-term trends analysis was performed on homogeneous time series, a substantial effort of quality
20 control, rupture detection and homogenisation (see Sect. 2.4) was performed in close collaboration with each station's PI on the data. As has been noted in previous papers, it is critical to have outside review of data to improve the quality of long-term time series (CC2013, Asmi et al., 2013). The final time series used in this analysis is available from following DOI: (*Doi will be created when the paper is accepted*).

25 The stations' environments were classified into four types (continental, coastal, mountain, or polar) that are represented by 22, 8, 16 and 7 time series, respectively. The type of measured aerosol at each site is further characterized by their footprints comprising 6 types (rural background, forest, desert, (sub)-urban, pristine and mixed). While the environments of Europe, North America and polar regions are fairly well represented, the number of long-term stations in
30 the rest of the world is currently quite low, resulting in a lack of information from the largest deserts (e.g. Sahara, Gobi, Australian, Arabian, Atacama), from many mountain ranges (e.g. Himalaya, Andes, Southern Great Escarpment, Great Dividiing Range, Ural) and from whole continents (South America (no site), Africa (one island in the Atlantic and one coastal site), and Australia (one coastal site)). Some stations from these underrepresented areas currently have 4 to 7 y of
35 measurements available and will potentially be used for trend analyses in the future (see table in Laj et al. (submitted)).

Sites were chosen based on the following criteria: (1) availability of at least 10 y of continuous data (two sites with 9 y and one site with 8 y of data for at least one parameter have also been included to improve spatial coverage (CPT, EGB and GSN, respectively)), (2) continuous
40 measurements without ruptures in the aerosol light scattering and/or absorption measurement; (3) submission of quality-assured data to the WMO WDCA data repository; (4) responsiveness of site operators to questions concerning data quality and homogeneity.

The longest time series with 40 y of measurements are the Arctic and Antarctic stations of BRW and SPO, followed by the high altitude MLO station (31 y). During the 1990's NOAA began
45 extending their network (Andrews et al., 2019), the IMPROVE network installed numerous stations in the USA (Malm et al., 1994), and the first long-term measurements in Europe, JFJ (Bukowiecki et al., 2016) and HPB, began in 1995. To have the largest representativity and to minimize the number of stations with less than 10 y of measurement, the current long-term trends were computed from time series ending in 2016, 2017 or 2018 (whichever year was most recently
50 available). To obtain an overview of the long term trend evolution in the past 40 y, all stations with at least 10 y of measurements were considered (see results Sect. 3.2).

2.2 Instruments

The relevant instruments operating at each site are listed in Table 1 and further instrument details are given in supplemental material (Table S1). Some particular instrumental features that could influence the trend analysis or comparison between stations are briefly discussed below.

5   Nephelometers measure aerosol light scattering over a truncated angular range (Müller et al., 2009 and references therein) leading to non-idealities often called "truncation error". The truncation adjustment accounts for scattering over the angles outside the measurement range and non-ideality of the light source. All TSI nephelometer scattering and backscattering sets were adjusted for truncation and instrument non-idealities using the Anderson and Ogren (1998)
10   correction. Thus, for times when enhanced amounts of large diameter (Dp>1 μm) particles are present, the measured scattering will be lower than true scattering by a substantial amount since the truncation correction increases with particle size (Anderson and Ogren, 1998, Molenar et al., 1997). The Radiance Research nephelometer has similar truncation characteristics as the TSI nephelometer (Müller et al., 2009). The Optec nephelometer measures over a wider angular
15   range (Molenar, 1997) than the other nephelometers and, like the Radiance Research measurements, the scattering has not been corrected for truncation in this study. The Optec nephelometers measure at ambient conditions with no size cut (they are open air instruments) so they can sample the very large particles present due to both hygroscopic growth at high humidities and/or the occurrence of precipitation, fog, dust, pollen, etc. The Ecotech nephelometers have a
20   similar angular range as the TSI nephelometers, and the measurements are corrected for truncation errors using the Müller correction (Müller et. al., 2011b), adapted from the Anderson and Ogren correction.

   For better comparability of aerosol properties amongst sites and to minimize the confounding effects of water associated with the aerosol, GAW recommends drying the sample air to RH<40%
25   (WMO/GAW report 227, 2016). While most of the nephelometer scattering time series are accompanied by sample RH measurements, this was not the case for all stations and for the entire measurement period. The calculated RH trends are therefore not always complete. Many breakpoints were detected in sample RH data and exchanges with the individual station PIs revealed that humidity sensors often suffer from artefacts, offsets, modifications that were not
30   considered as problematic. These sensor problems were often not resolved due to the secondary status of this housekeeping diagnostic leading to problematic time series. Nonetheless, apart from the IMPROVE network, the majority of nephelometers appeared to have sampled at RH<40%. The IMPROVE scattering measurements were analyzed at the measurement conditions with some constraints on acceptable scattering values, although the IMPROVE network recommends
35   screening the data when RH>90% (Prenni et al., 2019). For this study and according to CC2013, the IMPROVE scattering coefficient was restricted to σ_{sp} values lower than 500 Mm^{-1} for stations in the eastern USA (ACA, GSM, MCN and SHN) and lower than 100 Mm^{-1} for stations in the western USA to minimize the influence of rain, fog, snow and ice. These screening constraints minimized the issues associated with high RH but do not correspond to a screening on RH.

40   Measurement of the absorption coefficient was always performed by some type of filter-based photometer but relied on a variety of instruments. These instruments include: Multi-Angle Absorption Photometers (MAAP), Particle Soot Absorption Photometers (PSAP) and Continuous Light Absorption Photometers (CLAP), as well as various models of the Aethalometer (AE16, AE21, AE31 and AE33). All these instruments suffer from various artefacts, from which the
45   loading effect can influence the wavelength dependence. However, the largest uncertainty in filter-based photometer measurements lies in the effect of the multiple scattering of light into the filter matrix leading to over-prediction of absorption aerosol (e.g., Bond et al., 1999; Lack et al., 2008; Müller et al., 2011a; Collaud Coen et al., 2010, Bernardoni et al., 2019). This artefact is roughly corrected by the multiple scattering constant C_{ref}, and is probably the largest for the Aethalometer
50   and the smallest for the MAAP.

   The ACTRIS (European Research Infrastructure for the observation of Aerosol, Clouds and Trace Gases) community has suggested that Level 2 AE31 data submitted to EBAS utilize a multiple scattering constant C_{ref}=3.5; most of the analyzed AE31 time series were corrected with this new

rule. The AE33 adds a simultaneous measurement of the light transmission through a second filter spot sampling the same air at a different flow rate associated with a real-time compensation algorithm. This two spots technique allows for correction of the filter loading artefact. This improvement, however, has no effect on the largest artefact (multiple scattering artefact) and, as of yet, there is no agreed upon correction for the AE33 by the aerosol community. Previous AE models used a white light diode (AE10 and AE16) and a $C_{ref}= 1.6$ is usually applied. At FKL, the AE21 used a $C_{ref}=1.8$ and the AE33 a $C_{ref}= 3.0$. The various versions of the Aethalometer require then different corrections, whereas the real C_{ref} value depends on the filter and on the aerosol type. For background rural aerosol, the real C_{ref} value is between 2.5 and 4.5 (Collaud Coen et al., 2010, Bernardoni et al., 2019), the Asian plume has a relatively high C_{ref} between 4 and 5.5 (Kim et al., 2018), in the Arctic C_{ref} is suggest to be 3.45 (Backman et al., 2017), whereas pure mineral dust leads to lower C_{ref} of 1.75-2.56 (Di Biagio et al., 2017).

The MAAP measures not only the light transmission through the filter but also the light backscattered at two different angles. This design takes into account the scattering and multiple scattering artefacts (see Collaud Coen et al., 2010), which are two of the most significant artefacts for filter-based absorption photometers so that no correction is needed ($C_{ref}=1$). The MAAP measured absorption coefficient is consequently more reliable.

The CLAP was developed by NOAA as a replacement for the PSAP (Ogren et al., 2017). The CLAP was designed to have the same optical characteristics as the PSAP so that either the Bond et al. (1999) correction along with the Ogren (2010) update for wavelength and spot size correction or the Virkkula et al. (2005, 2010) corrections can be applied to account for scattering artifacts at multiple wavelengths as well other instrument non idealities (e.g., filter loading artefacts, variability in spot size and flow calibrations). These correction algorithms rely on co-located scattering measurements from a nephelometer and may have issues in the presence of large, primarily scattering aerosol such as sea salt or dust (e.g., Bond et al., 1999) and also may not work well when organic aerosol is abundant (e.g., Lack et al., 2008).

The differences in instrumentation, measurement conditions and post-processing data treatment do not allow the absolute values of aerosol optical parameters for all sites to be compared; however, because there was consistency of data treatment for each individual time series, the trends across the different sites can be compared.

2.3 Aerosol optical properties

The data used in this paper consist of hourly-averaged, quality-checked, spectral light scattering (σ_{sp}), backscattering (σ_{bsp}) and absorption (σ_{ap}) measurements. The quality checks correspond to the level 2 requirements of EBAS (Laj et al., submitted). After further visual quality control by the authors, the hourly data were aggregated into daily medians with the requirement that at least 25% of the daily data be valid. Such a low requirement for data coverage was chosen since 6 hourly measurements a day corresponds to half of the potential data coverage at many of the NOAA stations, where the operation mode consists of alternating between PM1 and PM10 size cutoff on a sub-hourly basis (Andrews et al., 2019).

All the nephelometers and the multi-wavelength absorption photometers measure at a green wavelength (~525-550 nm), which is the channel for which the parameters are reported. For the AE31 and AE33 models, the 520 nm channel was chosen. At several sites, the light absorption was measured by white light (~840-880 nm) Aethalometers (AE16), two channel Aethalometers (AE21) using 370 nm and 880 nm or by MAAPs (Multi-Angle Absorption Photometer) at 637 nm (Müller et al., 2011a), requiring the use of another wavelength, typically the red one. In some cases, the blue or red wavelength was preferred due to inhomogeneities or gaps in the green data. Since the trend analysis is not sensitive to the multiplication by a constant, the data series used to determine scattering and absorption trends were not adjusted to 550 nm.

In addition to the measured parameters, the following parameters were computed when the appropriate measurements were available:

- backscatter fraction, $b = \sigma_{bsp} / \sigma_{sp}$

- scattering Ångström exponent, $\mathring{a}_{sp} = -\ln(\sigma_{sp,1}/\sigma_{sp,2})/\ln(\lambda_1/\lambda_2)$

- absorption Ångström exponent, $\mathring{a}_{ap} = -\ln(\sigma_{ap,1}/\sigma_{ap,2})/\ln(\lambda_1/\lambda_2)$ or by a linear fit between the logarithm of the 7 absorption coefficients as a function of the logarithm of the 7 wavelengths of the Aethalometer (AE31 and AE33).

- single scattering albedo, $\omega_0 = \sigma_{sp}/(\sigma_{sp}+\sigma_{ap})$

where $\sigma_{sp,i}$ is the scattering coefficient at wavelength i, λ_i is the wavelength i, and σ_{bsp} is the hemispheric backscattering coefficient.

$\mathring{a}_{sp}$ and $\mathring{a}_{ap}$ were usually computed from the blue (~450 nm) and green wavelengths, because the red channel of the nephelometers was frequently less stable and more prone to rupture in
10 the time series due to calibrations or instrument changes. However, in some cases, other wavelength pairs were used to utilise the longest time series. $\mathring{a}_{ap}$ computed from the AE31 and AE33 is always more homogeneous if fitted on the 7 wavelengths, so that the fitted $\mathring{a}_{ap}$ was always chosen for these two instruments in this trend analysis.

The single scattering albedo was computed from σ_{sp} and σ_{ap} after σ_{ap} was adjusted to match the
15 nephelometer green wavelength with an assumed absorption Ångström exponent of one (i.e., $1/\lambda$ dependence). In order to maintain similar data treatment for absorption instruments with single or multiple wavelengths, the measured absorption Ångström exponents were not used for the wavelength adjustment for the ω_0 calculation.

It should be recalled that all parameters calculated using ratios of the σ_{sp} and/or σ_{ap} may have
20 higher uncertainties high for two reasons: (1) the ratio of two similar values has a larger uncertainty than the σ_{sp} or σ_{ap} uncertainties and (2) the σ_{sp} difference between the wavelengths depends on the nephelometer calibration that is performed independently for each wavelength. These largest uncertainties are particularly enhanced for clean locations with low aerosol loading.

In order to minimize the potential artefacts in the determination of the long-term trends in the
25 case of large seasonal variability (de Jong and de Bruin, 2012), only full start and end years of the time series, that is, without gaps in the data, were considered. For some stations, we did allow gaps of up to 4-6 weeks without measurements after checking that the removal of the whole year led to similar trend results.

2.4 Discontinuities, data consistency and homogenisation

30 Long-term climate analyses require homogeneous time series to be accurate. A homogeneous climate time series is defined as one where variations are caused only by variations in weather and climate (Conrad and Pollak, 1950) and in emissions of aerosol particles and their precursor gases. Long-term climatological time series can be affected by a number of non-climatic factors called breakpoints (e.g. relocation, instrument upgrades, inlet changes, calibrations, nearby
35 pollution sources) that mask the real climate variations. The breakpoints can be detected either by subjective visual inspection or by objective statistical methods (Peterson et al., 1998, Beaulieu et al., 2007) and must correspond to an event recorded in logbooks describing the station/instrumental history. Many statistical methods are only suitable for normally distributed data and cannot therefore be applied to aerosol optical properties measurement without data
40 transformation (Lindau and Venema, 2018). Moreover they are often applied not only to the data but to ratios or differences between various time series that are not systematically available at all the measuring sites of this study.

Visual inspection was used to detect breakpoints and to assess the validity of the time series to be used for climatic trend analysis. For this study, each measured and calculated (see Sect. 2.3)
45 parameter at all wavelengths, as well as all the possible ratios between measured parameters (including the number concentration if available), at each station were visually inspected in linear and logarithmic time series plots. The treatment of minimum and maximum values, of outliers and negatives along with the consistency of seasonal cycles were looked at closely when inspecting the time series plots. In addition, the data owners responded to a questionnaire about

potential break points, providing metadata that could be used to confirm/dismiss possible break points or to accurately locate them. The identified breakpoints were discussed with the data owners leading to corrections, homogenisation, invalidations or splitting of the time series into two parts. In one case (absorption data from SUM measured by AE16 and CLAP), the two time series were homogenised by multiplying the AE16 data by the median of the ratio between both data sets during the 10.5 months of simultaneous measurements. Only data sets considered as homogeneous by the authors and the data owners were analyzed in this study.

In the older networks, several modifications likely lead to inhomogeneities that occurred at sites in the network around the same time. Some of these include:

1) Two of the longest running NOAA stations changed their TSP (Total Suspended Particles) inlets for PM10 size cuts in the middle of the multi-decade time series (MLO: 2000, BRW: 1997). Some other stations outside the NOAA network also modified the measurement size cuts over their long-term measurement period. Usually this change of size cut (TSP to PM10) did not generate a break point for aerosol optical properties so that the time series could be considered as homogeneous. A differentiation between periods of sampling in- or outside of clouds was not made, even though TSP and PM10 could respond differently in these situations. In contrast, the modification of TSP or PM10 size cuts to PM2.5 or PM1 cutoffs usually led to visible breakpoints. PAL is the only station where changes between PM10, PM5 and PM2.5 did not induce a visually obvious breakpoint, likely due to the minimal presence of supermicron particles at this site.

2) The NOAA stations used the single green wavelength PSAP until the years 2005-2007 when they replaced them with a three wavelength (3w) PSAP (see Table S1). This instrumental change usually did not induce a visually obvious breakpoint.

3) A further instrument change for the absorption coefficient at NOAA sites occurred in 2013-2015 through the introduction of the 3w CLAP. The 3w PSAP to 3w CLAP change usually induced no breakpoint in the green absorption coefficient. The red channel sometimes exhibited a visible breakpoint (APP and BND), resulting in breakpoints in the absorption Ångström exponent. In those cases, calculation of the absorption Ångström exponent with the blue and green channels was preferred.

4) The long time series from MLO and JFJ were subject to the removal of negative values during the first years of measurements until 2000 and 1999, respectively. The raw data prior to these years were not archived by the data providers for either site. This change in minimal values does not seem to produce a clear breakpoint in the sense that the computed trends were not affected strongly enough to modify the climatic trends.

To compare long-term trends between stations from various networks, instruments and operators, instrumentation, measurement conditions and data treatment consistency is critical, but some lenience amongst stations was deemed acceptable. Specifically, some of the discretion was allowed including whether the data sets had the same corrections applied (e.g., truncation or not), how the sites dealt with sample RH and very low aerosol amounts, and inlet size cuts. Table 1 includes columns indicating information about the size cuts and RH conditions at the various sites. No screening or analysis as a function of cloud amount/clear sky conditions were done since these criteria/flagging were not available at all stations. Below, the impact of sample RH, size cut and of general instrument conditions and corrections on trend evaluation are briefly discussed:

1) Humidity: One important factor affecting all aerosol measurements is the relative humidity (RH) at which the measurements are made. For σ_{sp}, measurements at controlled RH enable minimization of the confounding effects of aerosol hygroscopic growth resulting in increases in the amount of scattering aerosol (Nessler et al., 2005, Fierz-Schmidhauser et al., 2010; Burgos et al., 2019). The disadvantage of making measurements at low RH is that aerosol hygroscopic properties must be measured or assumed in order to adjust the aerosol optical properties to ambient conditions. As noted above (see Sect 2.2), within the GAW program,

recommendations have been given to measure σ_{sp} at low (RH<40%) humidities. Apart from the IMPROVE and CPR nephelometers, the instruments typically operated at RH < 50%, with only six stations having a RH 95th percentile value larger than 50% (AMY, CMN, EGB, GSN, IPR and SGP) but with a median clearly much lower than 50%. In contrast, the IMPROVE network instruments measure at near ambient conditions (Malm et al., 1996). The scattering restriction method (see Sect 2.2) was chosen in order to maintain the highest data coverage - simply removing scattering values associated with RH>50% from the ambient IMPROVE data set would have eliminated most of the summertime measurements, particularly for the eastern USA locations. For all stations with some contribution of scattering made at RH values larger than 50%, the dry scattering and backscattering coefficients were calculated by removing values corresponding to hourly RH median >50%.

Ensuring a low humidity in the nephelometer reduces but does not suppress the potential influence of the hygroscopic growth on nephelometer measurements (Zieger et al., 2013). Therefore, if RH data were available, the RH long-term trends were also computed and their potential effect on the trend of σ_{sp}, σ_{bsp}, b and $\mathring{a}_{sp}$ was evaluated (see Sect 4.1).

The filter-based absorption photometers are also sensitive to rapid RH changes (e.g., Anderson et al., 2003), but daily absorption averages are usually not biased by such rapid fluctuations (Bernardoni et al., 2019). Very high sample RH could lead to higher uncertainties but absorption measurements at GAW stations are usually connected to inlets with some sort of conditioning intended to reduce sample RH (e.g. diffusion or membrane dryers, dilution with dry air and in some cases heating). Additionally, CLAPs are gently heated to ~37 C to minimize RH effects. In this study, stations with high sample RH in the nephelometer sample (Table 1) are also the most likely to have issues with high sample RH in the collocated absorption photometer.

2) Size cut: As described in Table 1, the size cuts differ amongst the stations, but most of the sites measure TSP or PM10. The GAW program generally recommends a PM10 size cut, except for stations in extreme environments (clouds etc.) where a whole air inlet is recommended (WMO/GAW report 227, 2016; GAW/WCCAP recommendations https://www.wmo-gaw-wcc-aerosol-physics.org/files/WCCAP-recommendation-for-aerosol-inlets-and-sampling-tubes.pdf). Many stations in the NOAA Federated Aerosol Network measure at a second size cut (PM1) as well. PAY and SUM are the only stations that have no measurement of coarse mode aerosol with only a PM2.5 inlet. As reported previously, the amount of aerosol particles larger than 10 micrometers is usually sufficiently low to enable consideration of TSP and PM10 results as in the same category. Moreover, the trend results of PM10 and PM1 sampling are found to be quite similar for all stations with both size cuts, so that the results of TSP/PM10 size cut will be presented in this study and, if not specified, PM1 results can be assumed to be similar to those of the larger size cut (PM10 or TSP).

3) Absorption filter photometers artefacts: The first main point to consider is that all filter-based absorption photometers suffer from various measurement artefacts and that continuous reference measurements to assess the absolute σ_{ap} values are not available at long-term monitoring sites. If the variability and the long-term trends of absorption coefficients are to be analysed with large confidence, the σ_{ap} absolute value is necessary to compute the ω_0. As stated in Sect 2.2, the real C_{ref} values can potentially vary by a factor of 4 (1.5 to 5.5). Using an erroneous C_{ref} value can influence the magnitude of the ω_0 trends. Similarly, an applied correction depending on the wavelengths can affect the absorption Ångström exponent calculation and its trends. Both ω_0 and $\mathring{a}_{ap}$ long-term trends therefore must be interpreted with greater care.

The differences in instrumentation, measurement conditions, and post-processing data treatment do not allow the absolute values for all sites to be compared; however, because there was consistency of data treatment for individual sites, the trends can be compared.

2.5 Trend analyses

The aerosol extensive parameters (σ_{sp}, σ_{bsp} and σ_{abs}) are not normally distributed and they exhibit varying degrees of autocorrelation. They can be represented approximately by a lognormal distribution but are usually better fitted by a distribution in the Johnson distribution family (Johnson, 1949). The intensive parameters (b, $\mathring{a}_{sp}$, $\mathring{a}_{ap}$ and ω_0) also exhibit distributions that differ to varying degrees from the normal distribution. We chose, therefore, to rely mostly on the non-parametric seasonal Mann-Kendall (MK) test associated with the Sen's slope. The MK test does not require normally distributed data. Additionally, as described under Sect. 2.5.1, the MK test was adapted to correctly handle autocorrelated datasets. To allow a comparison with other studies, the trends were also computed with the Generalized Least Squares analysis associated to the autoregressive or block bootstrap confidence intervals (GLS) and the least-mean square (LMS) fit applied to the data logarithms.

2.5.1 Mann-Kendall test and the Sen's slope estimator

This non-parametric method based on rank (Gilbert, 1987; Sirois, 1998) is the most appropriate test to compute optical properties trends because it can be applied regardless of missing values, statistical distribution and presence of negatives or below detection limits values in the data set. The MK test determines if a monotonic increasing or decreasing long-term trend exists, the slope and the confidence limits are then computed by the Sen's slope estimator that is based on the median of the slopes calculated from all possible data pairs. For this study, the MK test was applied on daily medians.

The MK test is designed for serially independent data and is consequently influenced by autocorrelation in the time series leading to inflated type I error; that is, there is increased probability of rejecting the no-trend hypothesis (i.e., a false positive). Several correction schemes for the MK test were proposed to correctly handle autocorrelated datasets and the problems induced by autocorrelation and its various corrections have been clearly described (Wang and Swail, 2001; Yue et al, 2002; Zhang and Zwiers, 2004; Bayazit and Önöz, 2007; Blain, 2013; Wang et al, 2015). A new method has been used for this study that tends to minimize the type I and II error (type II error is non-rejection of a false null hypothesis, i.e., a false negative) as well as the modification of the slope due to pre-whitening procedures by the application of three pre-whitening methods (Collaud Coen et al., in preparation). The standard pre-whitening (PW) by removing the first lag autocorrelation (von Storch, 1995) has a very low type I error but also a low test power, whereas the so-called trend-free pre-whitening procedure (TFPW) (Wang and Swail, 2001) restores the test power at the expense of the type I error. Both these PW procedures were applied prior to the MK test to assess the statistical significance of the trend. A trend was then considered as ss only if both PW procedures were ss at the 95% confidence level. Among the trends of all parameters at all stations calculated for this paper, none were ss for the PW but not for the TFPW, meaning that the PW procedure was always powerful enough. In contrast, many trends were not ss when PW was applied, but were ss with the TFPW procedure, showing that the TFPW rejection rate of the no-trend hypothesis is still too high.

After having determined the statistical significance, a third PW procedure, the variance-corrected TFPW allowing an increase in the slope accuracy (Wang et al., 2015) was applied prior to the Sen's slope estimation. The confidence limits of the Sen's slope were computed at the 90% confidence level.

Since many of the time series exhibited clear seasonal cycles, the modified seasonal MK test (Hirsch et al., 1982) was always applied to the four meteorological seasons. The overall trends were considered only if the slopes of the four seasons were homogeneous at the 90% confidence level.

Figure 2 presents three examples of seasonal MK results and Sen's slopes of σ_{sp}. At JFJ, σ_{sp} has ss negative overall trends for all of the analyzed periods, with the most recent 10 y period having a larger negative slope than the longer periods. Spring and autumn are the seasons at JFJ with the strongest trends and those trends are, mostly, statistically significant. MRN also exhibits σ_{sp}

overall negative trends for all of the analyzed periods, but only the 15 y, 20 y and 25 y trends are ss and their slopes are more negative for the longer periods. At MRN, summer and autumn are the seasons with the largest trends that remains constant for all the trend periods of all lengths (10 y to 25 y), while spring and winter have lower slopes for longer time periods. Finally, MLO has

5   negative overall trends that are not ss for the last 10 y and 15 y periods, whereas the 20 y, 25 y and 30 y periods exhibit ss positive trends. The spring season at MLO exhibits a not ss negative trend for the last 10 y and positive trends for the longest periods with only 25 y and 30 y trends being ss.

2.5.2 Least Mean Square analysis (LMS)

10 Following the Weatherhead procedure (Weatherhead et al., 2000), the trend is estimated by fitting the following frequently used statistical model for monthly data with an LMS approximation:

$$Y_t = m + C_t + \rho \cdot (t/12) + M_t, \qquad\qquad t = 1..n, \qquad\qquad (3)$$

where m is a constant term, C_t is a seasonal component, and ρ is the magnitude of the trend per year. The unexplained noise term M_t is modeled as an [AR(1)] process $M_t = \phi \cdot M_{t-1} + \epsilon$, where ϕ

15 is the autocorrelation coefficient of the data noise. For this study, either the logarithm of the monthly medians or the monthly medians were taken for all the parameters. Due to the non-normal distribution of the studied parameters, the LMS method applied on the logarithm is considered as the standard method according to previous trend analyses (CC2013 and Asmi et al., 2013). A trend is considered as ss at the 95% confidence level if $|\rho/\sigma_\rho| > 2$, σ_ρ being the

20 standard deviation of the slope. Fig. 3 a and c show the LMS trends and statistics for MLO σ_{sp}, respectively. The LMS results are similar to the MK analysis, the last 10 y trend are positive but ss at only the 90% confidence level, the 15 y and 20 y trends are not ss and the 25 y and 30 y trend are ss negative. The normal probability plot of the residue (Fig. 3c) shows that the use of the logarithm of the data results in normally distributed residues as required by this statistical tool.

25 ### 2.5.3 Generalized Least Square associated with autoregressive bootstrapping method (GLS/ARB)

A similar Generalized Least Squares (GLS) method based on the minimization of the least square errors similar to ordinary least squares fitting (including similar sensitivity to outliers), but taking into account the autocorrelation in the covariance matrix was also used in this study. The GLS

30 uses an autoregressive bootstrapping algorithm (ARB) to evaluate the potential differences in the GLS trends arising from the noise terms (Asmi et al., 2013). This ARB methodology was used to produce 1000 realizations of the original time series, with randomized noise terms, and the resulting set of trends was used to determine the 5th to 95th percentile confidence intervals (ARB CLs) of the GLS trends. If the ARB CLs did not include a zero trend, we considered the GLS trend

35 to be ss. The GLS and ARB methodologies were adapted from Mudelsee (2010) and applied to both daily and monthly medians. The previous trend analyses (CC2013 and Asmi et al., 2013) used daily medians.

Fig. 3b and f shows the GLS/ARB results for MLO σ_{sp} for daily and monthly medians. Here again the results are similar to the MK analysis, where the 10 y and 15 y are not ss while the longer

40 periods exhibit ss negative trends. As with many other stations included in this study, the use of daily or monthly medians did not result in normally distributed residues (Fig. 3f); and, in fact, the residues of the daily and monthly medians appeared to represent different types of distributions. It is also obvious that the seasonality fits (fits from monthly and daily medians in red and orange on Fig. 3b) are different for the two time granularities, with similar shape but higher absolute

45 values if fitted from daily medians. The timing of the winter minima is also more precisely defined with the daily data.

3. Results

3.1 Long-term trends ending in the present-day (2016-2018)

To globally assess the aerosol optical properties long-term trends, the largest number of stations around the world were included in this study. To satisfy this criterion, the overview takes into account the 10 y (or longer) trends ending in 2016, 2017 or 2018. The results shown here comprise not only the 10 y trends, but also the longer periods for 15 y to 40 y in 5 year increments also ending in 2016-2018. The results are presented for the MK analysis and a comparison between the trend analysis methods will follow in Sect. 3.3. Complete results for all the other methods can be found in the supplemental material.

3.1.1 Total scattering and hemispheric backscattering coefficients

Long-term trend analysis of σ_{sp} has been performed on 37 data sets. Since some nephelometers only measure σ_{sp} (Optec and Radiance Research nephelometers) and σ_{bsp} was determined to be unusable for several other sites due to various discontinuities (see Sect. 2.4), the hemispheric backscattering coefficient trends were computed on only 28 data sets. The detailed results of MK trend analyses are given in Table 2 while the overall picture for σ_{sp} is presented in Fig. 4. The results for σ_{bsp} are very similar to those for σ_{sp} for sites where both measurements existed; corresponding figures for σ_{bsp} can be found in the supplement material (Fig S1, S2 and S7).

The σ_{sp} ss trends are predominantly negative: 18 stations have ss negative 10 y trends, 5 stations ss positive trends and 14 stations no ss trends dispersed across all continents. Seven stations with time series longer than 10 y have ss negative 15 y trends and none of the 15 y trends are ss positive. The MK slopes range between -2.45 to +0.42 $Mm^{-1}y^{-1}$ with a mean of -0.31 $Mm^{-1}y^{-1}$. The main results are as follows:

- Over North America, all the σ_{sp} trends for periods longer than 10 y are ss negative and the most recent 10 y trends are generally ss negative. Four stations have not ss trends: (1) EGB's 9y time series does not allow for a ss trend (too short) but was included as one of only two Canadian sites, (2) MRN is an IMPROVE station on the west coast of the USA with very high humidity leading to condensation that can disturb the humidity measurement. This makes it difficult to know if the ss positive RH 10 y trend (Table S4) is real or due to measurement artefacts and uncertainties. If the ss positive RH trend is real, it could mask a decreasing σ_{sp} trend resulting in a not ss trend. The time coverage for the dry σ_{sp} (σ_{sp} restricted to RH<50%) for MRN is too low to be representative for trend analysis. It should be mentioned that the 10 y trends for MRN ending in 2014-2018 are all not ss (see Sect. 3.2.1) so that the absence of σ_{sp} trends seems to be a real phenomena. (3) RMN and GLR are also IMPROVE stations with high humidity. The RH trends at both stations are also not ss, the dry σ_{sp} has a ss negative trend, similar to other stations in its vicinity.

  In the previous decadal trend paper (CC2013), the trends in scattering for the arid state of Arizona were not consistent (ss positive: IBB, ss negative: SIA, PAZ, not ss: HGC, SCN). Four of the five Arizona sites (IBB, PAZ, SIA and SCB) were closed in 2010 and HGC now exhibits a ss decreasing scattering trend. MZW, the other IMPROVE station with ss positive scattering trends in 2010, also closed in 2010.

- Recent MLO 10 y and 15 y scattering trends are not ss, whereas the trends for the longer time periods (20-30 y) are ss positive (see Fig. 2). In the previous decadal trend paper (CC2013) MLO exhibited a ss positive trend for the 10 y period ending in 2010.

- Most (seven out of eleven) of the European sites have present day ss decreasing σ_{sp} trends. The other four stations have not ss trends: (1) one urban station also influenced by Saharan dust (UGR), (2) two sites in Eastern European countries (KPS and BEO) and (3) a high altitude station in the Central Range in France (PUY). The ss negative scattering trends of the Scandinavian stations have lower absolute slopes than in central Europe. PAL, the northernmost station, has a ss positive trend. PAL is geographically situated in

Europe but it can be climatologically considered to be an arctic station (Schmeisser et al. 2018). PAL (slope=0.06 Mm^{-1}/y) has a similar trend as ZEP (slope=0.05 $Mm.^{-1}./y$), the nearest Arctic station, with the largest ss trend in summer (JJA) when PAL is largely influenced by Arctic air masses. The increasing trend at PAL may be due to increasing biogenic secondary organic aerosol formation related to emissions from the surrounding boreal forest (Lihavainen et al., 2015), changes in circulation patterns or a larger influence of open water with increasing concentration of sea salt aerosol.

- Sites in polar regions exhibit the largest number of ss positive σ_{sp} trends. In addition to ZEP and PAL, SPO also has a ss positive present day 10 y trend but with lower slope, whereas no ss trends are found for two other polar sites (NMY and ALT). BRW has a ss negative 10 y trend, but longer periods of time lead alternatively to ss negative or not ss trends, with the longest periods exhibiting decreasing σ_{sp} trends. SPO also has very long time series with alternating trend slopes, from ss positive for the shortest periods (10-25 y) to ss negative for the longest periods (35-40 y), with some not ss trends in between. The aerosol load is very low at BRW, ZEP and SPO leading to scattering coefficients near the instrumental detection limits, so that the measurement uncertainties are proportionally larger than for middle latitude stations.

- Apart from polar regions and the continental GLR site, the only other ss positive trend is found for a site on the Caribbean island of Puerto Rico. At CPR, the largest scattering trend is found in summer and PM10 trends are five times larger than PM1. The most probable explanation is increased Saharan dust transport over the Atlantic ocean that was confirmed at the IMPROVE Virgin Island (Hand et al., 2017, Hand et al., 2019).

- The σ_{sp} trends are mostly (70%) not ss for stations at middle to high altitudes. From the 10 stations higher than 1100 m a.s.l., only SPO in Antarctica has a present day ss positive 10 y trend and only JFJ in the European Alps and HGC in Arizona exhibit ss negative 10 y trends. In contrast, only 26% of the stations lower than 1100 m a.s.l. have not ss trends. This difference can be due to the enhanced new particle formation and growth at high altitudes favored by the low temperatures and high solar radiation (e.g., Boulon et al., 2011; Rose et al., 2015) that increase the particle number concentration and the total scattering, and consequently mask potential decreasing σ_{sp} trends from anthropogenic pollution in the planetary boundary layer.

The seasonal MK results for σ_{sp} are presented in Fig. 5. MAM is the season with the largest number of ss decreasing trends and DJF with the lowest. ZEP and PAL exhibit ss positive trends only in JJA and BRW has ss negative trends only between December and May. The SPO annual trend is ss positive whereas it is not for NMY. Both Antarctic stations exhibit a coherent seasonality with ss positive trends only in MAM. While the 25 y and 30 y trends at MLO are all ss positive with the largest slope in spring when MLO is influenced by Asian long-range transport (CC2013), the most recent 10 y trend is decreasing in JJA and not ss for other seasons.

3.1.2 Absorption coefficient

The analysis of σ_{ap} long-term trends has been performed on 33 datasets (see Fig. 6 and Tables 2 and 3). The long-term trends are ss decreasing (20 stations) or not ss (12 stations) for all stations around the world except ALT. ALT has a slightly positive annual ss trend that is not consistent with the four seasonal trends observed at the site. ALT σ_{ap} is ss negative in spring and not ss (false positive results) but with positive slopes in all other three seasons. Moreover, the σ_{ap} trends at ALT are the only case where there is a strong discrepancy among the analysing methods, MK being ss positive, LMS/log not ss and GLS/day ss negative. The positive trend at ALT should thus be considered with great caution. The other main results are:

- In North America the number of σ_{ap} datasets is much lower than the number of σ_{sp} datasets (IMPROVE sites do measure aerosol absorption, but with a different instrumental setup (White et al., 2016)). From the five sites with long-term aerosol absorption, only APP and BND, both continental rural sites, have ss negative trends. The other three stations

representing continental rural US (SGP), marine west coast of the US (THD) and marine Caribbean island (CPR) environments exhibit not ss trends in σ_{ap}.

- In Europe, most (12 stations) of the 10 y σ_{ap} trends are ss negative. Only four stations, two in Scandinavia (BIR and PAL), one eastern continental high altitude (BEO) and one coastal Mediterranean (FKL) exhibit no ss trends. The 15 y σ_{ap} trend at JFJ is also ss negative.

- In Asia, only the high altitude station of LLN in Taiwan exhibits an annual ss decreasing σ_{ap} trend. The Chinese continental high altitude station of WLG and the coastal station of AMY have no ss annual trends.

- For polar regions, the Antarctica site of NMY, the American Arctic site of BRW and the Russian Arctic site of TIK have slight ss negative trends, whereas SUM and ZEP have no ss trends. Thus, there is no common clear σ_{ap} trend in polar regions.

- In the southwest Pacific, the high altitude station of MLO has a ss decreasing trend, whereas the coastal station of CGO in Australia exhibits not ss σ_{ap} trends.

- In contrast to the σ_{sp} trend, σ_{ap} trends at high altitude stations (> 1100 m a.s.l) are mostly (6 out of 8) ss decreasing, the trends at the other two high altitude stations are not ss.

The seasonal trends are more strongly negative and more ss in spring than in summer (see Fig S3). Winter is the season with the smallest number of ss decreasing trends in Europe (only 2/15), the others being not ss, whereas fall seems to be the season with the least ss trend in North America.

3.1.3 Single scattering albedo

As described under Sect. 2.4, ω_0 trends have to be considered with greater caution since the σ_{ap} absolute values suffer from a certain uncertainty related to filter-based absorption photometer artefacts.

The ω_0 trends depend directly on both the magnitude and the sign of the σ_{sp} and σ_{ap} trends. A σ_{ap} trend expressed in %/y larger (smaller) than the σ_{sp} trend will result in an increasing (decreasing) ω_0 trend, respectively (see Fig. S7 and related estimation of ω_0 uncertainty due to measurement and C_{ref} errors). The ω_0 trends are consequently much more diverse than the σ_{sp} and σ_{ap} trends with 52% of ss positive (relatively more scattering), 18% of ss negative (relatively more absorption) and 30% not ss trends (see Fig. 7). One peculiarity is that all ω_0 ss negative trends are found between latitude 30 and 50, but this is perhaps due to the low spatial coverage outside of North America and Europe. The main results are:

- The ω_0 is mostly decreasing in North America, where only APP and CPR have a ss positive ω_0 trend. The CPR ω_0 increasing trend can, perhaps, be related to increased Saharan dust load. The seasonal ω_0 trends at CPR are however ss not only in summer when Saharan influence is the greatest, but for every season except spring (Fig. 8). None of the other North America stations exhibits a ss trend in autumn and winter.

- European stations exhibit ss increasing ω_0 trends at the urban station of UGR and at most eastern and Scandinavian stations (KPS, SMR, PAL) and at HPB. These ss positive ω_0 trends in eastern Europe are the strongest in summer (Fig. 8), when MEL and BIR are also ss positive, and the weakest in winter when only PAL is ss positive (possibly related to increased particle formation from biogenic emissions, as mentioned above). In central Europe, JFJ, IPR and MSY have ss negative ω_0 trends for the entire year as well as for all seasons. PUY, a station at 1465 m in France's central range, has no ss overall trend due to a strong ss negative trend in summer and strong positive trends in autumn and winter. Because the site is located at a mid-range elevation (1465 m asl), PUY has a large probability of being influenced by different air masses as a function of the season, with a

large impact of the planetary boundary layer in summer (Collaud Coen et al., 2018; Hervo, 2013).

- The high altitude stations of LLN and WLG in Asia have a strong and a weak ss positive annual ω_0 trends, respectively, that is also observed for all seasonal trends at LLN but
  5   only in autumn at WLG. The coastal station of AMY has ss decreasing annual ω_0 trend that is due to decreasing trends in MAM and SON. AMY is located in an agricultural and touristic region that is influenced not only by these regional aerosol sources (e.g. traffic, field burning), but also by long-range transported plumes with high aerosol load.

- The two polar stations (BRW and NMY) exhibit no ss ω_0 annual trends, although there is
  10   a ss positive trend in summer at BRW for the most recent 10 y time series.

3.1.4 Backscattering fraction and scattering Ångström exponent

The present-day trends for b are mostly ss positive (61%) across all regions (Fig. 9). This suggests a shift in the size distribution towards smaller accumulation mode aerosol. The two
15 stations with ss negative trends are CPR in Puerto Rico and BEO, located on a summit in the Balkan range. Not ss trends are mostly found in eastern and northern Europe (KPS, MEL, BIR, PAL and SMR), in Antarctica (NMY 10 y trend and SPO 15 y trend), as well as at BND for the last 10 y. The Arctic sites have all ss positive b trends. CPR's seasonal trend is ss negative only in MAM (Spring), trends in b for the other seasons at CPR are not ss (see Fig S4). Similarly, the
20 BEO b seasonal trend is ss negative only in JJA, and not ss otherwise. PAL has ss positive b trend in spring and summer and ss negative b trends for autumn and winter leading to an annual not ss trend.

The scattering Ångström exponent ($å_{sp}$) trends exhibit a higher variability than the trends in other parameters. There are ss positive and negative trends in both North America and Europe and
25 the various trends cannot be attributed to specific regions or environments. The $å_{sp}$ trends seem to be more homogeneous in polar regions with either ss negative or not ss trends for the time periods with the exception of the 10 y trend at BRW. It should be recalled, however, that $å_{sp}$ is affected by higher uncertainties (see Sect 2.3) that may contribute to the larger variability observed for the $å_{sp}$ trends. The seasonal results also exhibit high variability, with winter being
30 the season with the least number of ss $å_{sp}$ trends (10 out of 26 sites), while spring is the season with the largest number of ss positive trends in $å_{sp}$ (8 out of 26 sites) (see Fig. S5).

3.1.5 Absorption Ångström exponent

The number of stations with long-term $å_{ap}$ measurement is low, with only 13 time series available. Six stations situated in various geographical regimes exhibit ss positive trends: polar regions (ALT
35 and ZEP), Atlantic coastal station (CPR), high altitude stations in the remote Pacific (MLO) and in continental Asia (WLG), and rural continental North American station (SGP). SMR and JFJ, two stations in Europe but with very different environmental footprints and altitudes, exhibit ss decreasing $å_{ap}$ trend, the six other stations, from which 4 coastal and 2 continental sites, have no ss trends.

40 While CPR, SGP and ALT $å_{ap}$ trends are ss positive for all four seasons, WLG is ss positive from June to February, MLO for summer and autumn and ZEP only for autumn (see Fig. S6). JFJ seasonal trends are all ss negative and SMR trends are ss negative in summer and autumn. The absorption Ångström exponent is principally a function of the particle chemical composition and material properties but its assignment to an aerosol type is not uniquely defined and also depends
45 on the particle size, with larger particles corresponding to lower $å_{ap}$ values (Liu et al, 2016, Schmeisser et al., 2017). For example, $å_{ap} >2$ corresponds to mineral dust in the case of big particles, and to brown carbon in the case of small particles. In contrast, $å_{ap} <1$ corresponds to large particles with small absorption like sea salt dominated aerosol in the case of big particles, and to BC dominated aerosol in the case of small particles. Following these observational
50 constraints, the JFJ and SMR aerosol tends to represent the category "mixed BC/BrC" according

Schmeisser et al. (2018). CPR absorption has a strong contribution from mineral dust and sea salt, whereas at MLO, SGP, ALT and ZEP contributions to absorption are from mixed sources including various light-absorbing carbon species and dust. Ideally, direct chemical composition measurements would provide more precise information on the aerosol type, but the necessary
5   chemical composition measurements are not yet readily available at many sites.

3.2 Time evolution of 10 year trends

The previous section describes the present day trends for different time periods extending from 10 y to 40 y. Another interesting analysis is to follow the evolution of the trends in time and space.
10   For this purpose, all the possible 10 y trends were computed and plotted as a timeline for each station. In what follows each point on the timeline represents a 10 y trend ending in the year it is located on the graph. For example, in Figure 12 the two black points for AMY represent the 10 y trends covering the periods 2008-2017 and 2009-2018, respectively. These timelines can be presented as a function of the latitude, longitude, altitude or environment. Depending on the
15   results, the most interesting representation has been chosen for each parameter.

3.2.1 Scattering and backscattering coefficients

Figure 12 presents the σ_{sp} 10 y trend timelines as a function of the longitude of the stations. The σ_{bsp} 10 y trend timelines are similar to the σ_{sp} trend timelines (see Fig. S7). The polar stations (in both the Arctic and Antarctic) have been gathered to the bottom of the figure just after the two
20   Pacific stations of MLO and CGO. The main result is that the sites in eastern and central North America (longitude between -68° and -112°) have ss negative σ_{sp} 10 y trends ending after 2010-2011 regardless of their altitude (200 to 2200 m a.s.l.) and their environments. This is a clear signature of continental scale modification due to air quality regulations and this very clear feature relates to the sulfate-dominated aerosol in the eastern US and to large SO_2 reductions in power
25   plants emissions (Hand et al., 2014, McClure and Jaffe, 2018). Almost all the σ_{sp} 10 y trends in the southwest US (MZW, SCN and HGC) ending before 2011 are ss positive as published in the previous trend analysis (CC2013). MLO also exhibits ss positive trends for the same period. These four stations are also high altitude sites (2000-3400 m) so that it is possible that all of them were influenced by long-range transport of highly polluted air masses from Asia (CC2013). It is
30   further interesting to note that the high altitude site JFJ (3580 m) in Europe also exhibited a ss positive 10 y trend ending in 2005-2007. Unfortunately, of all these high altitude stations, only MLO has a long enough σ_{ap} time series to compare with the ss positive σ_{sp} 10 y trends (Fig. 13). At MLO, the series of ss positive σ_{sp} 10 y trends ended in 2008, while the series of ss positive σ_{ap} 10 y trends occurred for the time period ending 2009-2012.

35   The evolution of the European σ_{sp} 10 y trends seems to be less homogeneous than in North America due to delays in abatement policies in each individual country. Apart PAL (which can be considered, to some extent, as a polar station), the σ_{sp} 10 y trends in Europe ending after 2008 are all ss negative or not ss. The four stations in Asia also have either ss negative or not ss trends ending in the last 5 years. The two African stations exhibit no ss trend. For polar sites,
40   BRW, ALT and NMY have mostly not ss trends, whereas SPO exhibits alternating ss positive and negative trends, with the oldest 10 y trends being not ss. In contrast, ZEP exhibits positive trends for all three 10 y groupings of scattering data at that site; which is similar to the 10 y trends at PAL for the same time periods. Due to the very low aerosol concentrations at these sites and, thus, larger measurement uncertainty, it is difficult to interpret the evolving σ_{sp} polar trends that
45   could relate to increased influence from the boreal forest and/or changed circulation patterns modifying the sea/ice influence.

The GSN dataset only covers 8 years with some missing periods due to the destruction of the station by a typhoon. Due to the very low number of long term measurements in Asia, GSN was included in this study. While GSN σ_{sp} summer trends are not reliable (low data coverage and
50   issues in humidity control), the ss negative winter-spring trends corresponding to the dry season

are valid and in line with the PM10 decreasing trends in Korea (Kim and Lee, 2018; Nam et al., 2018).

3.2.2 Absorption coefficient

The lengths of the σ_{ap} time series are much shorter than for σ_{sp} (Fig. 13). This means that the oldest 10 y trends cover the period 1998-2007 (BRW and BND), followed by MLO (2001-2010) and JFJ (2002-2011). For these four stations, the most recent 10 y trends are either not ss or ss negative. The present day (i.e., trends covering 2009-2018) ss negative 10 y trends (JFJ, BND) are preceded by not ss trends, whereas the present day not ss trends (MLO, SUM, BRW) are preceded by ss positive trends. Concerning MLO, it should be noted that both the σ_{sp} and σ_{ap} 10 y trends ending in 2018 are false positive decreasing trends based on the MK method and ss negative with both the GLS and LMS methods; the MLO PM1 σ_{ap} 10 y trend (not shown) ending in 2018 is also ss negative. The σ_{ap} 10 y trends evolution of each station is usually homogeneous with either ss negative or not ss 10 y trends in Asia, Europe, Africa and North America. Only polar stations and MLO exhibit some ss positive 10 y trends ending between 2010 and 2015. The length of the σ_{ap} time series is not long enough to detect other general features.

Figures 12 and 13 suggest that mid-latitude σ_{sp} and σ_{ap} sequential 10 y trends were ss positive for some periods between 2000 and 2010, followed by not ss trends and ending in the present day with ss negative trends. The evolution from increasing to decreasing σ_{sp} and σ_{ap} trends appears to be not simultaneous, with the σ_{sp} inflection points occurring some years before those for the σ_{ap} trends. The sparse number of stations with long enough time series does not allow generalisation of this result.

3.2.3 Single scattering albedo

Because it is limited by the length of σ_{ap}, time series, the ω_0 10 y trends evolution also only covers the last decade. The following results can be seen in Fig 14:

- All stations at longitude > 10° have ss positive ω_0 10 y trends except for MUK which exhibits a not ss 10 y trend ending in 2013. For European sites, ss positive ω_0 10 y trends exist for all stations at latitude >46.8° apart from BIR which has a not ss trend ending in 2018. This suggests that the decreasing σ_{ap} trends in Asia and in eastern and northern Europe are proportionally larger than the decreasing σ_{sp} trends.

- The central and western European sites exhibit ss negative or not ss ω_0 10 y trends. At JFJ and IPR, a shift between not ss to ss negative 10 y trends occurred in 2013-2014. The JFJ time series is moreover long enough to monitor ss positive ω_0 10 y trends ending in previous years (2011-2013). The urban station of UGR in Spain, exhibits an increasing trend in ω_0 (decrease in contribution of absorbing aerosol) for the most recent 10 y period (2009-2018), possibly relating to long-term effects of the 2008 financial crisis (e.g., Lyamani et al., 2011).

- In North America, the ω_0 10 y trends ending after 2013 are ss negative or not ss, apart from CPR in Puerto Rico. The sites with the longest series of ω_0 10 y trends (BND and THD) exhibit ss positive trends followed by not ss and ss negative trends. In contrast, MLO ω_0 10 y trends shifted from ss negative trends (10 y trends ending in 2010-2015) to not ss trends (10 y trends ending 2016-2018). This is in line with the observed increase of σ_{ap} 10 y trends ending in 2010-2012.

- The two polar sites of BRW and NMY exhibit mostly not ss ω_0 10 y trends, whereas ZEP, similar to PAL, exhibits ss positive ω_0 10 y trends.

3.2.4 Backscattering fraction and scattering Ångström exponent

Both the b and $\mathring{a}_{sp}$ 10 y trends in Asia and Africa exhibit similar 10 y trend patterns that are either ss positive or not ss (Fig. 15). In this context, similar means that the b and $\mathring{a}_{sp}$ trends are never ss when opposite signs of the slope are observed. These results suggest that particle average

size tends to decrease at the Asian and African sites. In Europe, b and $å_{sp}$ 10 y trends have a majority of ss negative or not ss trends in the northeast (longitude > 10°). At lower European longitudes, there is a discrepancy between b and $å_{sp}$ 10 y trends, with IPR, JFJ and PUY having opposite ss trends for b and $å_{sp}$, b trends being often ss positive and $å_{sp}$ trends often ss negative.

5 The discrepancy in the signs of the trends for b and $å_{sp}$ may be related to shifts in both the fine and coarse modes of the aerosol size distribution - this is discussed more below (see Sect. 4.2).

In North America, the b 10 y trends ending after 2012 are almost all ss positive whereas the previous 10 y trends are ss negative at BND and MLO. As in western America, one can see discrepancies in the sign of the slope for b and $å_{sp}$ 10 y trends, with APP, CPR, MLO, SGP and

10 THD having at least one 10 y period with opposite signed ss trends. Also, as in western Europe, the b trends are usually ss positive and the $å_{sp}$ trends ss negative. BND records four 10 y periods with opposite ss trends. In contrast to the other stations, BND $å_{sp}$ trends are ss positive while BND b exhibits ss negative trends.

In polar regions, the b 10 y ss trends ending after 2014 are all ss positive, whereas the older

15 trends are primarily ss negative. Here again, the discrepancy between b and $å_{sp}$ 10 y trends is large, with all the 10 y b and $å_{sp}$ trends for ZEP and ALT being ss with opposite signs. In contrast, BRW exhibits trends with the same sign for both parameters that can be interpreted as an increase of average particle size for early years followed by a decrease after 2014.

3.2.5 Absorption Ångström exponent

20 The $å_{ap}$ time series are not very long, because the first generation of absorption photometers used either white light or only one wavelength (Fig. 16). The longest time series of $å_{ap}$ begins in 2002 at JFJ and exhibits a continuous ss $å_{ap}$ decrease. Similar to the results for JFJ, most of the stations have consistently ss negative (JFJ, SMR), ss positive (ALT, CPR, MLO, SGP and WLG) or not ss 10 y trends (BRW, LLN and THD). Only ZEP and IPR exhibit changes in statistical

25 significance over the analysed period of time. The not ss trends of TIK and GSN may be due to datasets shorter than 10 y.

3.3 Comparison of the trends among methods

As described under Sect. 2.5, the long term trends were computed with three methods (MK, GLS and LMS), where GLS was used on both daily and monthly medians and LMS with and without

30 taking the logarithm of the monthly medians. These methods are thereafter called GLS/day, GLS/month, LMS/log and LMS/lin, respectively. Tables S2 and S3 give the GLS/day and LMS/log results for all parameters and stations. Table 3 presents an overview of the number of present day 10 y trends that are ss with each method. Due to the reasons described in Sect. 2.5.1, MK is considered as the most appropriate method for aerosol optical parameters. The agreement

35 between the three methods used in 2013, between all five methods are then also reported in Table 3, as well as the number of cases with either GLS/day or LMS/log agreement with MK and with both GLS/day and LMS/log disagreement with MK. The following conclusions can be derived:

- Generally, the trends computed by the various methods agree very well with another.
40 Among all parameters, all stations and all time periods, only one of the present-day trends presents ss results with opposite slope for different methods (10 y trend of the absorption coefficient at ALT, see Sect 3.1.2). In all the other cases, the differences among methods relates either to the degree of the ss or to the sign of the slopes for not ss trends. This implies that the main conclusions of this study would not have been fundamentally
45 different if the other methods were used.

- GLS applied on daily medians is the method that has the largest number of ss trends for all parameters.

- The three methods applied on monthly data have lower number of ss trends for all the computed parameters (ω_0, b, $å_{sp}$ and $å_{ap}$)

- The three methods used in 2013 have similar statistical significance (comprising cases with no ss trend) in 48% to 86% of the cases, whereas the five methods present a concordance in 40% to 82% of the cases. The measured parameters, which are less uncertain than the calculated parameters, always exhibit largest agreements amongst the methods (> 69% for the three methods used in 2013 and > 62% for the five methods utilized here). ω_0 is always the parameter with the largest dissimilarity among the methods and σ_{bsp} the parameter with the largest similarity between methods.

- The MK statistical significance is similar to at least one of the methods applied in 2013 in more than 90% of the cases for all of the parameters apart from ω_0 (88%) and $å_{ap}$ (78%). This lower level of agreement can be explained by the fact that ω_0 and $å_{ap}$ are almost normally distributed so that the use of the logarithm is not appropriate.

The boxplots of the slopes computed by the various methods (Fig. 17) show first that the application of the logarithm to transform to a normal distribution for ω_0 and $å_{ap}$ (not shown) is not suitable and leads to very large interquartile ranges. While the measured parameters are clearly not normally distributed, the computed parameters usually have distributions that more closely approximate normal distributions. No systematic rule could be deduced, since the distributions of each computed parameter largely depends on the individual stations. It seems however that ω_0 and the Ångström exponents are closer to the normal distribution than to the lognormal distribution.

The Sen slope estimator applied to the variance corrected prewhitening (Wang et al., 2015) leads, in almost all cases, to a median of the slope nearer to zero than the other methods. The variance-corrected TFPW method was developed specifically to get rid of the falsely increased slope by the trend free prewhitening process (Collaud Coen et al., in preparation). The LMS/log method sometimes results in lower absolute slope medians and this effect is probably due to the almost normal distribution of the data (= log of the monthly median). Both the GLS (GLS/day and GLS/month) and the LMS/lin method leads to higher absolute slopes, probably due to misuse of statistical methods derived for normally distributed data.

The GLS/day leads to broader range of slopes than the GLS/month. This larger variance can be due to (1) the larger variability of daily data leading to a less distinct seasonal cycle and, consequently, to a worse fit of the seasonal variation, and (2) a higher autocorrelation in the daily time series with probably an autocorrelation order larger than one.

4. Discussion

4.1 Considerations related to measurement humidity

As explained in the instrumental section, GAW protocol suggests that the σ_{sp} and σ_{bsp} be measured at low and controlled humidity, and that is the case for almost all stations considered here, except for those in the IMPROVE network which measure at ambient conditions due to their different monitoring goals. Temporal cycles and variations of RH with time are observed in a number of datasets. There are also some clear breakpoints in measurement RH that have been identified at several stations (e.g., an insulating jacket was installed on the nephelometer at THD in late 2012 resulting in a clear decrease in sample RH due to warmer nephelometer temperatures). It is evident that high RH will enhance particle diameters and, consequently, increase σ_{sp}, σ_{bsp} and ω_0 while resulting in decreased b and $å_{sp}$. This particle diameter enhancement depends not only on the RH values but also on the particle hygroscopicity, which is a function of the aerosol size distribution and chemical composition.

Similarly to the previous aerosol optical properties trend study (CC2013), dry σ_{sp} was calculated by removing data when measurement RH was higher than 50% in order to minimize the impact of aerosol hygroscopicity on the scattering trends. However, hygroscopic growth can occur for RH < 50%; for example, for sea salt aerosol, up to 25% of the scattering could be due to water at RH=40% (e.g., Figure 5 in Zieger et al. 2013). The confounding effects of aerosol water impact

the reported scattering values and, hence, the trends presented here to a greater or lesser extent. The effect of hygroscopic growth at RH<50% on the reported trends would depend on the temporal variability in sample RH, composition and size; investigating the interactions amongst those parameters is beyond the scope of this study.

5 For this study, if RH was frequently larger than 50% at a station, relationship between RH and aerosol parameters trends were analysed as follow. In the case of the RH trend being not ss, the aerosol parameters trends were considered to be independent of the RH variation. In the case where a ss RH trend was detected (see Table S4 in supplement), an attempt was made to try to determine the influence of RH trend on each aerosol parameter by considering the following

10 situations: (1) if all aerosol trends follow the RH trends, (2) if σ_{sp} at all measurement RH and dry σ_{sp} trends are similar, and, finally, (3) the features of σ_{ap} trends, which are less likely to be influenced by long-term RH variation. The distinct patterns exhibited by the evolution of the 10 y trends was very helpful in this analysis. Below we describe the assumed implications for scattering trends at sites where trends in RH were observed for several cases:

15 - Trends in RH are the opposite of both σ_{sp} and σ_{bsp} trends: this implies that the aerosol optical properties trends are real and not influenced by humidity (SMR, SHN, MRN)

- Trends in RH are ss but trends in σ_{sp} are not ss: this implies that the absence of statistical significance for the σ_{sp} trends is real if the slopes of the RH and σ_{sp} trend have the same sign (IZO, LLN) or can be partially induced by the RH trend if the slopes have opposite
20 signs (EGB, PUY, UGR)

- Trends in RH and σ_{sp} are similar, the overall and dry (RH<50%) σ_{sp} trends are similar, and σ_{sp} and σ_{ap} exhibit similar trends: This implies that the σ_{sp} trends are probably influenced by RH but also have an intrinsic aerosol trend (APP, BIR, MZW, SGP) .

- Trends in RH and σ_{sp} are similar, but the dry (RH<50%) and overall σ_{sp} trends are
25 dissimilar and the trends in σ_{sp} and σ_{ap} are also dissimilar: this implies that the RH influence is major (THD, CPR). THD and CPR are coastal stations with a dominant influence of sea salt. At THD on the North America west coast, RH, σ_{sp} and σ_{bsp} trends are ss decreasing, whereas b and $å_{sp}$ trends are ss increasing and σ_{ap} trends are also ss decreasing but with lower slope and ss than σ_{sp}. Further, the PM1 trends were less ss and
30 exhibited much lower slopes, suggesting that the large sea salt particles are probably sensitive to the RH decrease, leading to the decreasing σ_{sp} trend. The 10 y trends show that RH decreasing trends are particularly important until 2015 and likely explain the ω_0 ss positive 10 y trends ending in 2012 and 2013. At CPR, a coastal site in the Caribbean, RH, σ_{sp} and σ_{bsp} trends are ss increasing, but the σ_{ap} 10 y trends do not have the same
35 shape or statistical significance as the σ_{sp} trends. As observed at THD, the PM1 trends at CPR are less ss and have much lower slopes than PM10 trends.

As mentioned in the instrumental section, RH trends measured by the nephelometers have to be considered with caution. Because the measurement RH is only a secondary parameter, the instrument humidity sensors are typically not maintained or calibrated with the same care as the
40 scattered light detectors. The influence of humidity variations on the optical properties trends presented here can generally be considered as low, apart from the cases of very hygroscopic particles like sea salt (e.g., at THD and CPR). A better knowledge of the particle hygroscopic growth at low RH (< 40%) would be valuable in order to interpret σ_{sp} and σ_{bsp} trends as well as trends in ω_0, b and $å_{sp}$.

45 **4.2 Particle size trends**

Both the scattering Ångström exponent and the backscattering fraction are indicators of the particle's average size, with the general interpretation that lower values of b and $å_{sp}$ correspond to the presence of larger particles albeit at different parts of the aerosol size distribution (Collaud Coen et al., 2007). However, the relation between b and $å_{sp}$ is not uniquely defined for several
50 reasons. First, the scattering efficiency has an oscillating response to particle size rather than a constant increase. Second, the measured particle size distribution is usually composed of several

modes. Since the sensitivity of scattering to the mode depends on the size parameter (proportional to the ratio: diameter/wavelength), b (here usually taken at 550 nm) and å_{sp} (here usually computed with the 450-550 nm pair) do not always exhibit similar sensitivity to the various size modes. Further, the extinction Ångström exponent (analogous to å_{sp}) was found to be more

5   sensitive to fine mode volume fraction if computed from long wavelengths and to fine mode effective radius if computed from short wavelengths (Schuster et al., 2006). Lastly, the relation between b and å_{sp} also depends on the refractive index and consequently on the absorption coefficient (Hervo, 2013): for a constant particle diameter, an increase of the refractive index real part will decrease å_{sp} but increase b.

10   In this analysis, some stations exhibit b and å_{sp} trends with the same sign (BRW, CPT, SMR, LLN, SPO, UGR), while for other stations b and å_{sp} trends are in opposite directions (ALT, APP, BEO, BND, EGB, JFJ, MLO, MSY, PAL, PUY, SGP, SPO, ZEP). The plots showing the evolution of the 10 y trends (Fig 15) demonstrate that b and å_{sp} can exhibit either similar or opposite trends depending on the considered periods (CPR, IPR, MLO, THD). The plots showing the evolution of
15   the 10 y trends also suggest that the variations of the 10 y slopes are often identical in sign but different magnitude (e.g., shifted towards larger trend values for b (see for example MLO, Fig. 18)).

We can attribute both b and å_{sp} ss positive trends (ALT, BRW, SMR, LLN, THD, UGR) to a shift of the accumulation mode towards smaller sizes and a decrease of the coarse mode particle
20   concentration. In contrast, ss negative trends (BEO, CPR) for both b and å_{sp} suggest a shift to bigger sizes, specifically an increase in the coarse mode particle concentration and perhaps also a shift towards larger diameters of the accumulation mode. At a boreal forest site in northern Europe (SMR), size distribution data suggests that seasonal variation of b and å_{sp} was caused by a shift in the accumulation mode and not by changes in the coarse mode fraction (Luoma et al.,
25   2019). Trends towards smaller particle size might be due to an increase of near anthropogenic sources of pollution, to an increase in new particle formation, to a decrease of long-range transport of anthropogenic pollution or to increased scavenging of larger particles due to changes in atmospheric conditions. Trends towards bigger particles can relate to a decrease of near anthropogenic emissions, to larger influence of mineral dust caused by variation in desert
30   emissions or dust transport, to changes in agricultural activities or to an increase of humidity.

For stations with opposite b and å_{sp} trends, the chemical composition may play an important role in identifying reasons for the changing trends. It is however out of the scope of this paper to study these kind of dependencies.

4.3   Single scattering albedo trends

35   The single scattering albedo is the most important variable determining the direct radiative impact of aerosol so that its trend analysis - derived for the first time for a large number of stations - has a high relevance. The filter-based absorption photometers artefacts lead to uncertain absorption absolute values that have no effect on σ_{ap} trends but impart higher uncertainties to ω_0 trends. The results of ω_0 trends depend directly on the relative values of σ_{sp} and σ_{ap} trends. The global picture
40   is nuanced, with about half of ss positive, 1/5 of ss negative and a third of not ss trends leading to global positive median trend of 0.02%/y (Table 4). The median trends are increasing in Asia, in Arctic and in the Pacific, but decreasing in Europe and North America. The largest median slopes are found in Asia and in the Pacific (+0.12%/y), whereas the decreasing median slopes are relatively small (< 0.1%/y). The beginning of the decrease of the aerosol burden varies with
45   region; the earliest decrease is found in Europe in the 1980's (Tørseth et al., 2012), followed by North America in the 1990's (Bodhaine and Dutton, 1993) and by Asia some 10-15 years ago (Sogacheva et al., 2019, Zhao et al., 2019). The median slope of the ω_0 trends seems to be proportional to the length of the mitigation efforts, which for some relevant pollutants (e.g., black carbon, SO_2 and NO_x) are still ongoing. In Europe, the diversity of the timing of abatement policies
50   with earlier impact in western Europe than in Eastern Europe (Vestreng et al., 2007, Crippa et al., 2016, Huang et al. 2017) is also directly visible in the decreasing and increasing ω_0 trends, respectively.

These results suggest that policy regulations induced first a ω_0 increase (global cooling effect) and, in a second phase, a ω_0 decrease (global warming effect). The Emission Database for Global Atmospheric Research (EDGAR V4.3.2) (easy accessible via https://eccad.aeris-data.fr/) shows that both the black carbon (BC) and SO_2 emissions decreased rapidly during the 1990s, and that
5   currently emission reductions of SO_2 are larger than the reductions for BC. From this we conclude that the reduction of primary particles, such as BC, leads first to the ω_0 increase, whereas the reduction of SO_2, a precursor of secondary particle formation, tends to result in a ω_0 decrease. This different timing and evolution in primary and secondary aerosol concentrations could explain the evolution of the 10 y ω_0 trend at IPR, JFJ, BND and THD (Fig. 14) but the time series are not
10   long enough to properly assess this change.

These observed ω_0 trends are in line with the modelled impact of aerosol on climate (Zhao et al., 2019). They found a global cooling effect of -0.41K due to growth of aerosol burden caused by an increase in energy use in the northern hemisphere (particularly in Asia) is counterbalanced by a global warming of +0.10 K caused by the decreased aerosol emissions due to technology
15   advances particularly in North America and Europe. This illustrates the complex nexus of environmental pollution regulations which have positive effects for health and the environment (air pollution is a primary cause of premature deaths in much of the world, Landrigan et al., 2018) but may have an adverse effect on efforts to reduce climate change. Ideally, abatement policy would take into account both climate and health impacts.

20   **4.4 Comparison with other trends and causality**

When comparing present day trends to 2010 trends (CC2013), it is obvious that the larger number of stations, particularly in Europe, permits a more detailed view of regional trends. The ss decreasing σ_{sp}, σ_{bsp} and σ_{ap} trends in North America observed in CC2013 for time series ending in 2010 are found to have continued in this work. The current wide coverage across continental
25   Europe also shows decreasing present-day trends. Decreasing trends of extensive aerosol properties were confirmed for different analysis periods for PAL (Lihavainen et al., 2015) with the further result that the trends do not depend on the air mass origin, TIK (Davuliene et al., 2019) for equivalent black carbon (eBC) trends, SMR (Luoma et al., 2019), BND and SGP (Sherman et al., 2015) and JFJ, HPB, IPR, IZO, PAL, PUY, SMR and UGR (Lyamani et al., 2011; Pandolfi et al.,
30   2018). Some disagreements are also found between this study and Pandolfi et al. (2018) that seem to be principally due to the analyzed periods - three more years included in this study and some older periods of data included in Pandolfi et al. (2018) were invalidated in this study following the evaluations described in Sect. 2.4. A decreasing trend in black carbon (BC) concentration is also found in Europe (Singh et al., 2018; Kutzner et al., 2018; Grange et al., 2019) that has been
35   related primarily to traffic emission decreases rather than changes in wood burning and/or industrial emissions. Mean absorption coefficient (estimated from light transmittance measurements on 24 h filter samples) at the 110 IMPROVE stations was also found to decrease for the 2003-2014 period (White et al., 2016), but with a smaller slope than the elemental carbon trend which is due to the impact of Fe content in mineral dust. The European b and $\mathring{a}_{sp}$ trends
40   computed by Pandolfi et al. (2018) are similar to the results of this study for most of the stations, in that they also found a general ss increase of b and variable $\mathring{a}_{sp}$ trends. SPO σ_{sp}, b and $\mathring{a}_{sp}$ trends for the 1979-2014 period (Sheridan et al., 2016) do agree with CC2013 results, whereas the 1979-2018 trends reported in this study suggest an evolution towards more ss positive trends. The very low aerosol concentrations in Antarctica and the difference in the MK algorithm could
45   however also explain the differences.

The main cause of trends in both aerosol intensive and extensive properties is likely strong reduction of both primary aerosols and precursors of secondary aerosol formation due to continental to regional mitigation strategies. These reductions of anthropogenic emissions are also measured in PM masses in US (Hand et al., 2019), in Europe (Pandolfi et al., 2016) and in
50   airborne (Sogachova et al., 2019; Li et al., 2017) and ground-based (Zhao et al., 2019; Ningombam et al., 2019) Aerosol Optical Depth (AOD) measurements. Ningombam et al. analysed AOD 1995-2018 trends from 53 remote and high altitude sites, of which 21 had ss negative trends. The results of the few sites involved in both studies are similar for LLN, MLO (not ss trends) and SPO (ss increasing), but different for IZO (no ss trends for in situ extensive

parameters but ss decreasing AOD), BRW and BIR (ss decreasing in-situ trends but not ss AOD trends). It should be noted that trends in the integral of the ambient extinction coefficient over the atmospheric column (AOD) should not necessarily be expected to be comparable to the low RH surface in-situ σ_{sp}, σ_{bsp} and σ_{ap}, and, further, that the analyzed time period and the trend analysis
5   methods are different. Yoon et al. (2016) sees decreasing trends in AOD over the US and Europe, although they note an increase in extreme events in the western US which they hypothesize could be due to wildfires. McClure and Jaffe (2018) confirmed an increase of $PM_{2.5}$ 98 percentiles in Northwest US due to an increase in wildfires superimposed on the global decrease in anthropogenic emissions. Yoon et al. (2016) observe larger decreasing trends in AOD in Europe
10   than in the US, which is also the case in this study (see Table 4) but with small differences. Yoon et al. (2016) also notes that there is a lack of measurements in many regions similar to the lack of representativeness in the surface in-situ aerosol sites discussed in this study (Asia, Africa, South America, etc).

Zhao et al. (2019) attribute the AOD, ω_0 and $\mathring{a}_{sp}$ decreases in North America and Europe to
15   considerable emission reductions in all major pollutants except in mineral dust and ammonia, so that these reductions are visible in the small size fraction but not in large size (>1.4 µm) non spherical aerosols. The largest decreases are found in summer in the eastern US and in spring and summer in the Western Europe, whereas minimal decreases occur in autumn and winter in the US and only winter in Europe. These seasonal column aerosol trends are consistent with the
20   σ_{ap} and (to a large extent) the σ_{sp} trends (see Sect. 3.1.2 and 3.1.1) found in this study. Li et al. (2017) showed that the decrease in West and central Europe is principally due to sulfate, whereas in Eastern Europe the organic aerosol also plays a role. The simulation of the emission reductions due to abatement policy (Crippa et al., 2016) resulted in the largest $PM_{2.5}$ decreases in Europe and North America between 1970 and 2010. Pandolfi et al. (2016) found decreasing trends for
25   many PM compounds and sources at both Barcelona and MSY in NE of Spain. The sources that showed statistically significant downward trends during 2004–2014 were secondary sulfate, secondary nitrate, and heavy oil combustion sources. Ealo et al. (2018) have shown that the aforementioned sources at MSY had very high mass scattering efficiencies compared to other sources. Pandolfi et al. (2016) also showed statistically significant decreasing trends for the
30   contributions to PM from the industrial/traffic source at MSY (mixed metallurgy and road traffic) and from the industrial (metallurgy mainly) source at Barcelona (less efficient scatterers as reported in Ealo et al. (2018)). These sources were clearly linked with anthropogenic activities, and the observed decreasing trends confirmed the effectiveness of pollution control measures implemented at European or regional/local levels. Conversely, at regional level, the contributions
35   from sources mostly linked with natural processes such as aged marine and aged organics did not show statistically significant trends.

In Asia, the rapid economic growth led to increased AOD between 1980 and 2010 (Butt et al., 2017, Yoon et al., 2016), but significant decreases are now measured and modelled in the last decade in South East Asia (Sogacheva et al., 2019). In contrast, ss increasing AOD trends are
40   found at remote and isolated sites in Asia, in high altitude Himalayan regions, in the southern hemisphere ocean and in Antarctica. Zhao et al. (2019) explained the observed AOD decrease in China since 2011 by an effective reduction in anthropogenic emissions in autumn and minimal reductions in winter. The PM2.5 mass is found to continuously increase in some part of Asia (e.g., in India) for the 1989-2013 period principally due to increases in organic aerosol and secondary
45   inorganic aerosol, whereas the increases in BC, nitrate and ammonium are comparably moderate (Li et al., 2017). These trends reflect the extensive agriculture and the high-energy consumption of the residential sector. In China, similar to AOD, the PM2.5 trend presents a transition from increasing to decreasing trend in 2006-2008. However, the AOD was still found to increase with no reduction of PM2.5 in megacities and heavily industrialized areas in East Asia due to
50   continuous primary fine particle emissions and secondary particle formation (Nam et al., 2018). The in-situ measurements in China presented in this study are however not long enough to reflect this change.

Similar results are found for sulphate trends (Aas et al., 2019) with decreasing trends across Europe and the US, albeit with the decrease in Europe happening first. They describe potential

increases in sulfate in India and increases followed by decreases in SE Asia. Vestreng et al. (2007) monitored the SO_2 emission reduction in Europe and concluded that their reductions were largest in the 1990s with a first decrease in Western Europe in the 1980s followed by a large decrease in Eastern Europe in the 1990s. Similarly Crippa et al. (2016) simulate a larger impact

5   of policy reduction in Western than in Eastern Europe for NO_x, CO, PM_{10} and BC between 1970 and 2010. Likewise, Huang et al. (2017) simulated the non-methane volatile organic compounds emissions and found a rapid decrease in Europe and in North America since the 1990s, whereas the emission of Africa and Asia clearly increased between 1970 and 2012. It should be noted that the difference in NO_x, NMVOC, SO_x, NH_3, CO, $PM_{2.5}$ and PM_{10} emission trends between Western

10   and Eastern Europe is becoming more significant since 2010 (EMEP status report, 2019). While slowly decreasing emissions are reported in the Western part of the EMEP domain, the estimated increasing emissions of all pollutants since 2000 in the Eastern part are mainly influenced by emission estimates for the remaining Asian areas in the EMEP modelled domain.

    While it is beyond the scope of this effort to explore in depth the causes of the observed trends of

15   aerosol optical properties, some general comments can be made. The main causes all around the world appear to relate mostly to changes in anthropogenic emissions. Long-range transport is also a key influence at particular sites such as the Saharan dust impact at CPR, IZO and UGR, North African pollution due to developing industries at IZO, and the Asian pollution at the high altitude station of MLO. Mountainous stations can also be affected by modifications of the

20   planetary boundary layer or of the continuous aerosol layer heights responding to ground temperature or mesoscale synoptic weather changes. The number and intensity of wildfires has increased in several regions and particularly in the western US (Hand et al., 2014). While this may eventually lead to noticeable trend effects at some of the sites in this study, wildfire influence is probably more visible in the maxima than in the median values used here (McClure and Jaffe,

25   2018). Climate change also affects soil drought and the positive feedback between drought and wildfires can also affect aerosol optical properties (Hallar et al., 2017, McClure and Jaffe, 2018). The trend sign oscillation at BRW is potentially caused by the very low aerosol concentration, but the effects of atmospheric oscillations such as El Nino or to sea ice coverage cannot be excluded. Similarly, the seasonality of SPO trends could also be interpreted as a modification of the Antarctic

30   polar vortex temporality or intensity.

    Detailed studies at each station are however necessary to discriminate between direct causes like changes in anthropogenic emissions, and indirect causes bounded to general climate changes such as soil drought, ground albedo and temperature, sea ice coverage or atmospheric circulation pattern. The availability of the homogenized data set from this study will provide a

35   useful tool for these types of analyses.

5. Conclusion and recommendations

    This second long-term trend analysis of in-situ aerosol measurements derived from stations with large spatial representation leads to a more coherent picture of aerosol radiative properties

40   around the world. Results from this study provide evidence that the aerosol load has significantly decreased over the last two decades in the regions represented by the 52 stations. The mean extensive property trends are decreasing for all parameters (σ_{sp}, σ_{bsp} and σ_{ap}) and all regions apart from the σ_{sp} trend in the South Pacific and in polar regions (see Table 4). These decreases in aerosol burden are assumed to be a direct consequence of decreases in primary particles and

45   particulate precursors such as SO_2 and NO_x due to pollution abatement policies. This assumption is supported by trend results for the USA where the inflection point between not ss and ss decreasing σ_{sp} 10 y trends consistently occurred over the same time period (2010-2011) for all central and eastern stations. While the overall σ_{ap} decrease (-2.5 to -5%/y for the ss trends in all regions) is larger than that for σ_{sp}, the σ_{ap} time series are not long enough to detect the beginning

50   of σ_{ap} decreasing 10 y trends.

The single scattering albedo trend analysis - derived for the first time from a large number of stations - has the largest climatic relevance. The uncertainty of the ω_0 trend is larger than for the other aerosol parameters due to the possible error in absorption coefficient absolute value. The global picture is nuanced with ss positive trends mostly in Asia and Eastern Europe and ss negative in Western Europe and North America leading to global positive median trend of 0.02%/y. It appears that the historical abatement policies for gaseous species and primary aerosol particles (e.g., in Western Europe in the 1980s) have resulted in present-day decreasing ω_0 trends in the western hemisphere, whereas more recent regulations (Asia) are leading to increasing ω_0 trends. For example, the absorption coefficient may be largely reduced in a first phase (e.g., due to regulations on primary emissions) whereas the scattering coefficient is more impacted in a second phase (regulations on aerosol precursors). Again, this suggests it is necessary to consider how regulatory policies designed to improve health and environmental outcomes impact climate change efforts and vice versa.

The backscattering fraction and scattering Ångström exponent trends relate mostly to the average particle size distribution and to the relative concentrations in the accumulation and coarse modes of the size distribution, but the mean refractive index also plays a role. The interpretation of the results for these parameters is less straightforward as, depending on the site, the trends for b and $å_{sp}$ may have the same or opposite sign. The causes of particle size change encompass not only the primary aerosol emission but also the emission of secondary aerosol precursors, the particle chemistry and condensation rate, the hygroscopic growth and the humidity condition during the measurement. In general, the interpretation of b, $å_{sp}$ and $å_{ap}$ trends is more difficult, and the effects of global climate change on aridity, wildfire frequency and intensity, planetary boundary layer height, transportation patterns or natural oscillation must also be investigated in order to find the causality of aerosol optical properties changes.

This study was limited by the lack of information from many WMO regions. Since 2010, the number of stations with time series longer than 10 y has doubled (24 in 2010, 52 currently) so that the spatial coverage is improved and various additional environments are covered in Europe, North America and in polar regions. A first result of this study is that, while aerosol exhibits a very weak spatial and temporal homogeneity, general features can be deduced with the present station density in Europe and North America, while the picture in polar regions is less clear. The few stations in Asia, Africa, South America and in Oceania/Pacific region cannot, however, be considered as representative for their continents/regions, first, because of their small number and, second, because mountainous and coastal environments are overrepresented relative to the continental environment with rural, forest or desert footprints. According to information from the GAWSIS metadata base, more stations located in underrepresented regions are now in operation, which promises a better spatial coverage in a few years, however, sustaining these operations is still an open issue (the longest time series in India closed in 2016) and not all stations are actually providing their data in open access, with the proper associated metadata. Even in developed countries, the financial resources needed to operate long-term monitoring are not always secure, leading to the closing of stations, to a decrease of time series quality and/or to a delay in data submission to the international data banks.

Furthermore, in this study, a number of datasets were not used or were only partially used due to the occurrence of break points following instrumental or inlet changes or even calibration shifts. High quality data rely on attention to international recommendations for measurements, on a regular maintenance schedule, participation in inter-comparison efforts and on high-level quality control. The existence of metadata, logbooks and station's history is crucial for determining causes of any detected break points and necessary to enable the generation of a final homogenized time series for trend analysis. This homogenization process provides us with an important finding: a critical review of the data by others outside the measurement network is very important in improving the quality of the reported data. This study has resulted in a large improvement to the EBAS database and in the quality of the reported datasets.

Based on the results of this study and with a view toward future trend analyses, the following recommendations concerning the improvement of aerosol optical time series are raised:

- The station history, metadata and logbooks have to be detailed and handled with great care, since they are absolutely necessary to evaluate long-term trends on homogenized time series.

- Time series are affected not only by the instrument type or inlet changes, but also by replacement by instruments of the same type and by shifts in calibrations.

- A rotation between instruments in a network (e.g., to enable repairs) will decrease potential missed data losses but has a potential to increase breakpoints in the time series, particularly in the wavelength dependence of the parameters.

- The scattering and backscattering coefficients and the backscattering fraction and the scattering Ångström exponents are very sensitive to the humidity conditions in the nephelometers due to the hygroscopic growth of particles even at low RH. The nephelometer humidity sensors should be better checked and characterized in order to assess long-term trends of dry particles.

- Long-term trend analysis should not be computed on time series shorter than 10 y, since short datasets lead to a larger probability of false or not ss trend detection due because of the low number of elements in the time series.

- Stations with long-term records have to be sustained and their funding should be assured in order to study the future impact of aerosol on climate change. Stations maintenance as well as new station creation in regions with a low spatial coverage (Africa, South America,
20
Asia and Oceania) should be particularly encouraged.

Data availability: Almost all datasets are available as level 2 NASA/AMES files at EBAS (http://ebas.nilu.no/) at an hourly resolution. The screened datasets used for this study aggregated as daily medians can be found at DOI:...

25   *Author contribution*: CLM, YL and EA gathered datasets and applied additional QC to the time series. MCC did a further QC, computed the long-term trends and analysed the results. MCC and EA wrote the manuscript. NB, JH, PL, CLM, MP, and PZ extensively contributed to the revision of the manuscript. All the other co-authors contribute to the measurements of aerosol optical properties at the 52 stations and to the manuscript reviewing.

30   *Competing interests*: The authors declare that they have no conflict of interest.

Acknowledgements

The authors would like to thank the numerous, but unfortunately unnamed, technical and scientific staff members of the stations as well as many students included in these analyses, whose dedication to quality for decades have made this paper possible. Provision of data from this study
35   have mainly been acquired in the framework of NOAA-FAN (https://www.esrl.noaa.gov/gmd/aero/net/); ACTRIS, under the ACTRIS-2 (Aerosols, Clouds, and Trace gases Research InfraStructure) project supported by European Union (grant agreement no. 654109); and IMPROVE (http://vista.cira.colostate.edu/Improve/). Some European sites and measurements were also supported by the Co-operative Programme for Monitoring and
40   Evaluation of the Long-range Transmission of Air pollutants in Europe (EMEP) under UNECE. The authors also gratefully acknowledge the following persons and organizations:

- AMY: the Korea Meteorological Administration Research and Development Program "Development of Monitoring and Analysis Techniques for Atmospheric Composition in Korea" under Grant (1365003041).
45   - APP: Appalachian State College of Arts and Sciences, electronics technician Michael Hughes, machinist Dana Greene

- BEO: projects ACTRIS2 and ACTRIS-BG
- BIR: the project no 80026 Arctic Monitoring and Assessment Programme (AMAP) under the EU-action "Black Carbon in the Arctic". Aerosol optical/physical properties at Birkenes II are financed by the Norwegian Environment Agency

5 - CGO: the Australian Bureau of Meteorology for their long term and continued support of the Cape Grim Baseline Air Pollution Monitoring Station, and all the staff from the Bureau of Meteorology and CSIRO, particularly John Gras who instigated the measurements of aerosol scattering and absorption
- CPR: Para La Naturaleza and the nature reserve of Cabezas de San Juan and the support of
10 grants AGS 0936879 and EAR-1331841.
- GSN: the Basic Science Research Program through the National Research Foundation of Korea (2017R1D1A1B06032548).
- SMR: the European Union Seventh Framework Programme under grant agreement No 262254. This research has also received funding from the European Union's Horizon 2020 research and
15 innovation programme under grant agreement No 654109 via project ACTRIS-2 and grant agreement No 689443 via project iCUPE. The work was also funded by the Academy of Finland (project. No 307331).
- IMPROVE: IMPROVE is a collaborative association of state, tribal, and federal agencies, and international partners. Support for IMPROVE nephelometers comes from the National Park
20 Service. The assumptions, findings, conclusions, judgments, and views presented herein are those of the authors and should not be interpreted as necessarily representing the National Park Service (stations: ACA, BBE, CRG, GBN, GLR, GSM, HGC, MCN, MRN, MZW, NCC, RMN, SCN, SHN).
- IZO: Measurement Programme within the Global Atmospheric Watch (GAW) Programme at the
25 Izaña Atmospheric Research Centre, financed by AEMET.
- JFJ: Urs Baltensperger, Günther Wehrle, Erik Herrmann; the International Foundation High Altitude Research Station Jungfraujoch and Gornergrat (HSFJG), the Swiss contributions (GAW-CH and GAW-CH-Plus) to the Global Atmosphere Watch programme of the World Meteorological Organization (WMO) which are coordinated by MeteoSwiss; in the context of ACTRIS: the
30 European Union's Horizon 2020 research and innovation programme under grant agreement no. 654109 (ACTRIS-2 project) and no. 739530 (ACTRIS-PPP project), as well as the Swiss State Secretariat for Education, Research and Innovation, SERI, under contract number 15.0159-1 (ACTRIS-2 project). The opinions expressed and arguments employed herein do not necessarily reflect the official views of the Swiss Government.
35 - LLN: the Taiwan Environmental Protection Administration for their continued support of the Lulin Atmospheric Background Station (LABS); the Ministry of Science and Technology for the support to individual PIs' research funding.
- MSY: the European Union's Horizon 2020 research and innovation programme under grant agreement no. 654109, ACTRIS (project no. 262254), ACTRIS-PPP (project no. 739530).
40 Measurements at MSY (Montseny) station was supported by the MINECO (Spanish Ministry of Economy, Industry and Competitiveness) and FEDER funds under the PRISMA project (CGL2012-39623-C02/00) and under the HOUSE project (CGL2016-78594-R), by the MAGRAMA (Spanish Ministry of Agriculture, Food and Environment) and by the Generalitat de Catalunya (AGAUR 2014 SGR33, AGAUR 2017 SGR41 and the DGQA). Marco Pandolfi is
45 funded by a Ramón y Cajal Fellowship (RYC-2013-14036) awarded by the Spanish Ministry of Economy and Competitiveness.
- MUK: the Ministry of Foreign Affairs of Finland, project grants (264242, 268004, 284536, and 287440) received from Academy of Finland; Business Finland and DBT, India sponsored project (2634/31/2015), the Centre of Excellence in Atmospheric Science funded by the Finnish Academy
50 of Sciences (307331), and an esteemed collaboration of FMI and TERI.
- NOAA stations (BND, BRW, MLO, SGP, SPO, SUM, THD): Derek Hageman for all his programming efforts for NOAA and NFAN stations, John Ogren for initiating the expanded NFAN measurements and NOAA's Climate Program Office for funding
- PAY: the Swiss Federal Office for the Environment (FOEN).
55 - PUY: the staff of OPGC and LaMP, INSU-CNRS and the University Clermont Auvergne, and the financial support from ACTRIS-France National Research infrastructure and CNRS-INSU long-term observing program..

- SGP: the U.S. Department of Energy Atmospheric Radiation Measurement Program via Argonne National Laboratory, the DOE SGP ARM Climate Research Facility staff and scientists.
- TIK: The Aethalometer was supplied by Russ Schnell; Tiksi overall logistics and operations by Taneil Uttal and Sara Morris (NOAA/ESRL/PSD, Boulder, CO, USA).
5   - UGR: the European Union's Horizon 2020 research and innovation program through project ACTRIS-2 (grant agreement No 654109), the Spanish Ministry of Economy and Competitiveness through projects CGL2016-81092-R, CGL2017-90884-REDT and RTI2018-101154-A-I00.
– WLG: China Meteorological Administration for their continued support to Waliguan Atmospheric Baseline Station; National Scientific Foundation of China (41675129), National Key Project of
10 Ministry of Science and Technology of the People's Republic of China (2016YFC0203305 & 2016YFC0203306), Basic Research Project of Chinese Academy of Meteorological of Sciences (2017Z011). It was also supported by the Innovation Team for Haze-fog Observation and Forecasts of China Meteorological Administration.
- ZEP: the Swedish EPA's (Naturvårdsverket) Environmental monitoring program
15 (Miljöövervakning), the Knut-and-Alice-Wallenberg Foundation within the ACAS project (Arctic Climate Across Scales, project no. 2016.0024), the research engineers Tabea Henning, Ondrej Tesar and Birgitta Noone from ACES and the staff from the Norwegian Polar Institute (NPI), NPI for substantial long-term support in maintaining the measurements, Maria Burgos and Dominic Heslin-Rees (ACES) for preparing the data.

References

Aas, W., Mortier, A., Bowersox, V., Cherian, R., Faluvegi, G., Fagerli, H., Hand, J., Klimont, Z., Galy-Lacaux, C., Lehmann, C. M. B., Lund Myhre, C., Oliviè, D., Sato, K., Quaas, J., Rao, P. S. P., Schulz, M., Shindell, D., Skeie, R. B., Stein, A.,Takemura, T., Tsyro, S., Vet, R. and Xu,
25   X.: Global and regional trends of atmospheric sulfur, Scientific Reports, *9*(1), 1–11. https://doi.org/10.1038/s41598-018-37304-0, 2019.

Anderson, T. L. and Ogren, J. A.: Determining aerosol radiative properties using the TSI 3563 integrating nephelometer, Aerosol Sci. Tech., 29, 57–69, 1998.

Anderson, T. L., Masonis, S. J., Covert, D. S., Ahlquist, N. C., Howell, S. G., Clarke, A. D., and
30   McNaughton, C. S.: Variability of aerosol optical properties derived from in situ aircraft measurements during ACE-Asia, J. Geophys. Res., 108, 8647, doi:10.1029/2002JD003247, 2003.

Andrews, E., Sheridan, P., Ogren, J.A., Hageman, D., Jefferson, A., Wendell, J., Alastuey, A., Alados-Arboledas, L., Bergin, M., Ealo, M., Hallar, A.G., Hoffer, A., Kalapov, I., Keywood, M.,
35   Kim, J., Kim, S.-W., Kolonjari, F., Labuschagne, C., Lin, N.-H., Macdonald, A., Mayol-Bracero, O.L., McCubbin, I.B., Pandolfi, M., Reisen, F., Sharma, S., Sherman, J. P., Sorribas, M., Sun, J.: Overview of the NOAA/ESRL Federated Aerosol Network, Bull. Amer. Meteor. Soc., 100, 123-135, doi:10.1175.BAMS-D-17-0175.1, 2019.

Asmi, A., Collaud Coen, M., Ogren, J. A., Andrews, E., Sheridan, P., Jefferson, A., Weingartner,
40   E., Baltensperger, U., Bukowiecki, N., Lihavainen, H., Kivekas, N., Asmi, E., Aalto, P. P., Kulmala, M., Wiedensohler, A., Birmili, W., Hamed, A., O'Dowd, C., Jen- nings, S. G., Weller, R., Flentje, H., Mari Fjaeraa, A., Fiebig, M., Lund Myhre, C., Hallar, A. G., Swietlicki, E., Kristensson, A., and Laj, P.: Aerosol decadal trends – Part 2: In-situ aerosol particle number concentrations at GAW and ACTRIS stations, Atmos. Chem. Phys., 13, 895–916,
45   doi:10.5194/acp-13-895-2013, 2013.

Backman J., Schmeisser, L., Virkkula, A., Ogren, J.A., Asmi, E., Starkweather, S., Sharma, S., Eleftheriades, K., Uttal, T., Jefferson, A., Bergin, M., Makshtas, A., Tunved, P., Fiebig, M.: On Aethalometer measurement uncertainties and multiple scattering enhancement in the Arctic, Atmos. Meas. Tech., 10, 5039-5062, doi:10.5194/amt-10-4039-2017, 2017.

Bayazit, M., and Önöz, B.: To prewhiten or not to prewhiten in trend analysis? Hydro. Sci., *52*(4), 611–624, https://doi.org/10.1623/hysj.53.3.669, 2007.

Bernardoni, V., Ferrero, L., Soldan, F., Valentini, S., Massabo, D., Mocnik, G., Gregoric, A., Cataldi, M., Bolzacchini, E., Prati, P., Valli, G. and Vecchi, R.: Multi-wavelength aerosol absorption coefficient measurements: instrument intercomparison and results of source and component modelling, poster, European Aerosol Conference, Göteborg, Sweden, 25-30 September 2019, 2019.

Beaulieu, C., Ouarda, T.B.M.J., and Seidou, O. : Synthèse des techniques d'homognénéisation des séries climatiques et analyse d'applicabilité aux séries de précipitations, Hydro. Sci., 52(1), 2007

Blain, G. C.: The modified Mann-Kendall test: on the performance of three variance correction approaches. Bragantia, *72*(4), 416–425, https://doi.org/10.1590/brag.2013.045, 2013.

Bodhaine, B. A.: Aerosol absorption measurements at Barrow, Mauna Loa and the South Pole, J. Geophys, Res,: Atmospheres, 100(D5), 8967–8975. https://doi.org/10.1029/95JD00513, 1995.

Bodhaine, B. A., and Dutton, E. G.: A long-term decrease in arctic haze at Barrow, Alaska, Geophys. Res. Lett., 20(10), 947–950, 1993.

Bond, T. C., Anderson, T. L., and Campbell, D.: Calibration and intercomparison of filter-based measurements of visible light absorption by aerosols, Aerosol Sci. Tech., 30, 582–600, doi:10.1080/027868299304435, 1999.

Boulon, J., Sellegri, K., Hervo, M., Picard, D., Pichon, J. M., Fréville, P., & Laj, P.: Investigation of nucleation events vertical extent: A long term study at two different altitude sites, Atmos. Chem. Phys., *11*(12), 5625–5639, https://doi.org/10.5194/acp-11-5625-2011, 2011.

Bukowiecki, N., Weingartner, E., Gysel, M., Collaud Coen, M., Zieger, P., Herrmann, E., Steinbacher, M., Gäggeler, H. W. and Baltensperger, U.: A review of more than 20 years of aerosol observation at the high altitude research station Jungfraujoch, Switzerland (3580 m asl), Aerosol Air Qual. Res., https://doi.org/10.4209/aaqr.2015.05.0305, 2016.

Burgos, M., Andrews, E., Titos, G,, Alados-Arboledas, L., Baltensperger, U., Day, D., Jefferson, A., Kalivitis, N., Kouvarakis, G., Mihalopoulis, N., Sherman, J.P., Sun., J., Weingartner, E., and Zieger, P.: Data Descriptor: A global view on the effect of water uptake on aerosol particle light scattering, Scientific Data, 6,157, https://doi.org/10.1038/s1597-019-0158-7, 2019.

Butt, E. W., Turnock, S. T., Rigby, R., Reddington, C. L., Yoshioka, M., Johnson, J. S., Regayre, L. A., Pringle, K. J., Mann, G. W. and Spracklen, D. V.: Global and regional trends in particulate air pollution and attributable health burden over the past 50 years, Environ. Res. Lett., 12(10). https://doi.org/10.1088/1748-9326/aa87be, 2017.

Choi, M., Lim, H., Kim, J., Lee, S., Eck, T. F., Holben, B. N., Garay, M. J., Hyer, E. J., Saide, P. E., and Liu, H.: Validation, comparison, and integration of GOCI, AHI, MODIS, MISR, and VIIRS aerosol optical depth over East Asia during the 2016 KORUS-AQ campaign, Atmos. Meas. Tech., 12, 4619–4641, https://doi.org/10.5194/amt-12-4619-2019 , 2019.

Collaud Coen, M., Andrews, E., Asmi, A., Baltensperger, U., Bukowiecki, N., Day, D., Fiebig, M., Fjaeraa, A. M., Flentje, H., Hyvärinen, A., Jefferson, A., Jennings, S. G., Kouvarakis, G., Lihavainen, H., Lund Myhre, C., Malm, W. C., Mihapopoulos, N., Molenar, J. V., O'Dowd, C., Ogren, J. A., Schichtel, B. A., Sheridan, P., Virkkula, A., Weingartner, E., Weller, R. and Laj, P.: Aerosol decadal trends-Part 1: In-situ optical measurements at GAW and IMPROVE stations, Atmos. Chem. Phys. 13, 869–894. https://doi.org/10.5194/acp-13-869-2013, 2013.

Collaud Coen, M., Andrews, E., Bisi, A., et al. in preparation.

Collaud Coen, M., Andrews, E., Aliaga, D., Andrade, M., Angelov, H., Bukowiecki, N., Ealo, M., Fialho, P., Flentje, H., Hallar, A. G., Hooda, R., Kalapov, I., Krejci, R., Lin, N.-H., Marinoni, A., Ming, J., Nguyen, N. A., Pandolfi, M., Pont, V., Ries, L., Rodríguez, S., Schauer, G., Sellegri,

K., Sharma, S., Sun, J., Tunved, P., Velasquez, P., and Ruffieux, D.: Identification of topographic features influencing aerosol observations at high altitude stations, Atmos. Chem. Phys., 18, 12289–12313, https://doi.org/10.5194/acp-18-12289-2018, 2018.

Collaud Coen, M., Weingartner, E., Apituley, A., Ceburnis, D., Fierz-Schmidhauser, R., Flentje, H., Henzing, J. S., Jennings, S., G., Moerman, M., Petzold, A., Schmid, O., Baltensperger, U.: Minimizing light absorption measurement artifacts of the Aethalometer: Evaluation of five correction algorithms, Atmos. Meas. Tech. https://doi.org/10.5194/amt-3-457-2010, 2010.

Collaud Coen, M., Weingartner, E., Nyeki, S., Cozic, J., Henning, S., Verheggen, B., Gehrig, R., and Baltensperger, U.: Long-term trend analysis of aerosol variables at the high-alpine site Jungfraujoch, J. Geophys. Res., 112, D13213, doi:10.1029/2006JD007995, 2007.

Conrad, V. and Pollak, L.W.: Methods in Climatology, Harvard University Press, Boston, 1950.

Crippa, P., Sullivan, R. C., Thota, A., and Pryor, S. C.: Evaluating the skill of high-resolution WRF-Chem simulations in describing drivers of aerosol direct climate forcing on the regional scale, Atmos. Chem. Phys., 16, 397–416, https://doi.org/10.5194/acp-16-397-2016, 2016.

Davuliene, L., Sakalys, J., Dudoitis, V., Reklaite, A., and Ulevicius, V.: Long-term black carbon variation in the South-Eastern Baltic Region in 2008–2015, Atmos. Poll. Res., 10(1), 123–133. https://doi.org/10.1016/j.apr.2018.06.013, 2019.

De Jong, R., and De Bruin, S.: Linear trends in seasonal vegetation time series and the modifiable temporal unit problem, Biogeosciences, 9(1), 71–77, https://doi.org/10.5194/bg-9-71-2012, 2012.

Di Biagio, C., Formenti, P., Cazaunau, M., Pangui, E., Marchand, N., and Doussin, J.-F.: Aethalometer multiple scattering correction Cref for mineral dust aerosols, Atmos. Meas. Tech. 10, 2923–2939. https://doi.org/10.5194/amt-2017-65, 2017.

Boulon, J., Sellegri, K., Hervo, M., Picard, D., Pichon, J. M., Fréville, P., and Laj, P.: Investigation of nucleation events vertical extent: A long term study at two different altitude sites, Atmos. Chem. Phys., 11(12), 5625–5639. https://doi.org/10.5194/acp-11-5625-2011, 2011.

Ealo, M., Alastuey, A., Pérez, N., Ripoll, A., Querol, X., and Pandolfi, M.: Impact of aerosol particle sources on optical properties in urban, regional and remote areas in the north-western Mediterranean, Atmos. Chem. Phys., 18, 1149–1169, https://doi.org/10.5194/acp-18-1149-2018, 2018.

EMEP Status Report 2019: Transboundry particulate matter, photo-oxidants, acidifying and eutrophying components, ISSN 1504-6109 (print) ISSN 1504-6192 (on-line), 2019.

Fierz-Schmidhauser, R., Zieger, P., Gysel, M., Kammermann, L., DeCarlo, P. F., Baltensperger, U., & Weingartner, E.: Measured and predicted aerosol light scattering enhancement factors at the high alpine site Jungfraujoch, Atmos. Chem. Phys., 10(5), 1–26, 2010.

Gilbert, R. O.: Statistical Methods for Environmental Pollution Monitoring, Van Nostrand Reinhold Company, New York, 1987.

Grange, S. K., Lötscher, H., Fischer, A., Emmenegger, L., and Hueglin, C.: Evaluation of equivalent black carbon (EBC) source appointment using observations from Switzerland between 2008 and 2018, Atmos. Meas. Tech. Discuss., https://doi.org/10.5194/amt-2019-351, in review, 2019.

Hallar, A. G., Molotch, N. P., Hand, J. L., Livneh, B., McCubbin, I. B., Petersen, R., Michalsky, J., Lowenthal, D. and Kunkel, K. E.: Impacts of increasing aridity and wildfires on aerosol loading in the intermountain Western US, Environ. Res. Lett. 12(1), 1–8, https://doi.org/10.1088/1748-9326/aa510a, 2017.

Hand, J. L., Gill, T. E., and Schichtel, B. A.: Spatial and seasonal variability in fine mineral dust and coarse aerosol mass at remote sites across the United States, Journal of Geophysical Research, 122(5), 3080–3097, https://doi.org/10.1002/2016JD026290, 2017.

Hand, J. L., Gill, T. E., and Schichtel, B. A.: Urban and rural coarse aerosol mass across the United States: Spatial and seasonal variability and long-term trends. Atmospheric Environment, 218(October), 117025, https://doi.org/10.1016/j.atmosenv.2019.117025, 2019.

5   Hand, J. L., Schichtel, B. A., Malm, W. C., Copeland, S., Molenar, J. V., Frank, N., and Pitchford, M.: Widespread reductions in haze across the United States from the early 1990s through 2011, Atmos. Environ., *94*, 671–679. https://doi.org/10.1016/j.atmosenv.2014.05.062, 2014.

Hand, J.L., Prenni, A.J., Schichtel, B.A., Malm., W.C., and Chow, J.C.: Trends in remote PM2.5 residual mass across the United States: Implications for aerosol mass reconstruction in the IMPROVE network, Atmos. Environ., 203, 141-152, 2019.

10   Hervo, M. : Etude des propriétés optiques et radiatives des aérosols en atmosphère réelle : Impact de l'hygroscopicité. Sciences de la Terre. Université Blaise Pascal - Clermont-Ferrand II, ⟨NNT : 2013CLF22337⟩, 2013.

Hirsch, R. M., Slack, J. R., and Smith, R. A. : Techniques of trend analysis for monthly water quality data, Water Resour. Res., 18,107–121, 1982.

15   Huang, G., Brook, R., Crippa, M., Janssens-Maenhout, G., Schieberle, C., Dore, C., Guizzardi, D., Muntean, M., Schaaf, E., and Friedrich, R.: Speciation of anthropogenic emissions of non-methane volatile organic compounds: a global gridded data set for 1970–2012, Atmos. Chem. Phys., 17, 7683–7701, https://doi.org/10.5194/acp-17-7683-2017, 2017.

Intergovernmental Panel on Climate Change, and J. T. Houghton. *IPCC First Assessment Report*.

20   Geneva: WMO, 1990.

IPCC: Working Group I Contribution to the IPCC Fifth Assessment Report Climate Change 2013: The Physical Science Basis, Summary for Policymakers, IPCC, Geneva, Switzerland, Final Draft pp., 2013.

Johnson, N. L., Systems of frequency curves generated by methods of translation, Biometrika,

25   36, 149–176, 1949.

Kim, J-H., Kim, S-W., Ogren, J.A., Sheridan, P.J., Yoon, S-C., Sharma, S., and Lin, N-H.: Multiple scattering correction factor estimation for aethalometer aerosol absorption coefficient measurement, Aerosol Sci. Technol., doi:10.1080/02786826.2018.1555368, 2018.

Kim, Y. P., and Lee, G.: Trend of air quality in Seoul: Policy and science Aerosol and Air Quality

30   Research, 18(9), 2141–2156, https://doi.org/10.4209/aaqr.2018.03.0081, 2018.

Kutzner, R. D., von Schneidemesser, E., Kuik, F., Quedenau, J., Weatherhead, E. C., and Schmale, J.: Long-term monitoring of black carbon across Germany, Atmos. Environ., 185, 41–52, https://doi.org/10.1016/j.atmosenv.2018.04.039, 2018.

Lack, D. A., Cappa, C. D., Covert, D. S., Baynard, T., Massoli, P., Sierau, B., Bates, T. S., Quinn,

35   P. K., Lovejoy, E. R., and Ravishankara, A. R.: Bias in Filter-Based Aerosol Light Absorption Measurements Due to Organic Aerosol Loading: Evidence from Ambient Measurement, Aerosol Sci. Tech., 42, 1033–1041, 2008.

Laj, P. et al., "A global analysis of climate-relevant aerosol properties retrieved from the network of GAW near-surface observatories" , submitted.

40   Landrigan, P.J., Fuller, R., Acosta, N.J.R., Adeyi, O., Arnold, R., Basu, N., Baldé, A., Bertollini, R., Bose-O'Reilly, S., Boufford, J.I., Breysse, P.N., Chiles, T., Mahidol, C., Coll-Seck, A.M., Cropper, M.L., Fobil, J., Fuster, V., Greenstone, M., Haines, A., Hanrahan, D., Hunter, D., Khare, M., Krupnick, A., Lanphear, B., Lohani, B., Martin, K., Mathiasen, K.V., McTeer, M.A>, Murray, C.J.L., Ndahimananjara, J.D., Perera, F., Potočnik, J., Preker, A.S., Ramesh, J.,

45   Rockström, J., Salinas, C., Samson, L.D., Sanilya, K., Sly, P.D., Smith, K.R., Steiner, A., Stewart, R.B., Suk, W.A., van Schayck, O.C., Yadama, G.N., Yumkella, K., and Zhong, M: The Lancet Commission on pollution and health, The Lancet, 391, 462-512, https://doi.org/10.1016/S0140-6736(17)32345-0, 2018.

Li, C., Martin, R. V., Boys, B. L., Van Donkelaar, A., and Ruzzante, S.: Evaluation and application

50   of multi-decadal visibility data for trend analysis of atmospheric haze, Atmos. Chem. Phys., 16(4), 2435–2457. https://doi.org/10.5194/acp-16-2435-2016, 2016.

Li, C., Martin, R. V., Van Donkelaar, A., Boys, B. L., Hammer, M. S., Xu, J. W., Marais, E. A., Reff, A., Strum, M., Ridley, D.A., Crippa, M., Brauer, M., and Zhang, Q.: Trends in Chemical Composition of Global and Regional Population-Weighted Fine Particulate Matter Estimated for 25 Years, Environ. Sci. Tech., 51(19), 11185–11195. https://doi.org/10.1021/acs.est.7b02530, 2017.

Lihavainen, H., Asmi, E., Aaltonen, V., Makkonen, U., Kerminen, V-M., Direct radiative feedback due to biogenic secondary organic aerosol estimated from boreal forest site observations, Environ. Res. Lett., 10, 10.1088/1748-9326/10/10/104005, 2015.

Lihavainen, H., Hyvärinen, A., Asmi, E., Hatakka, J., and Viisanen, Y.: Long-term variability of aerosol optical properties in northern Finland, Boreal Environ. Res., 20(4), 526–541, 2015.

Lindau, R., ans Venema, V. K. C.: The joint influence of break and noise variance on the break detection capability in time series homogenization, Advances in Statistical Climatology, Meteorology and Oceanography, 4(1/2), 1–18. https://doi.org/10.5194/ascmo-4-1-2018, 2018.

Liu, C., Chung, C. E., Zhang, F., and Yin, Y.: The colors of biomass burning aerosols in the atmosphere, Scientific Reports, 6, 1–9. https://doi.org/10.1038/srep28267, 2016.

Luoma, K., Virkkula, A., Aalto, P., Petäjä, T., and Kulmala, M.: Over a 10-year record of aerosol optical properties at SMEAR II, Atmos. Chem. Phys., 19, 11363–11382, https://doi.org/10.5194/acp-19-11363-2019, 2019.

Lyamani, H., Olmo, F.J., Foyo, I., Alados-Arboledas, L.: Black carbon aerosols over an urban area in south-eastern Spain: changes detected after the 2008 economic crisis. Atmos. Environ., 45, 6423-6432, 2011.

Malm, W.C., Sisler, J.F., Huffman, D., Eldred, R.A., Cahill, T.A.: Spatial and seasonal trends in particle concentration and optical extinction in the United States, J. Geophys. Res., 1347-1370, DOI: 10.1029/93JD02916, 1994.

Malm, W. C., Molenar, J. V., Eldred, R. A., and Sisler, J. F.: Examining the relationship among atmospheric aerosols and light scattering and extinction in the Grand Canyon area, J. Geophys. Res., 101, 19251–19265, 1996.

McClure, C. D., and Jaffe, D. A.: US particulate matter air quality improves except in wildfire-prone areas, Proceedings of the National Academy of Sciences of the United States of America, 115(31), 7901–7906. https://doi.org/10.1073/pnas.1804353115, 2018.

Molenar, J. V.: Analysis of the real world performance of the Optec NGN-2 ambient nephelometer, Visual Air Quality: Aerosols and Global Radiation Balance, Air and Waste Management Association, Pittsburgh, 243–265, 1997.

Mudelsee, M.: Climate Time Series Analysis, vol. 42 of Atmospheric and Oceanographic Sciences Library, Springer, Heidelberg, 2010.

Müller, T., Henzing, J. S., de Leeuw, G., Wiedensohler, A., Alastuey, A., Angelov, H., Bizjak, M., Collaud Coen, M., Engström, J. E., Gruening, C., Hillamo, R., Hoffer, A., Imre, K., Ivanow, P., Jennings, G., Sun, J. Y., Kalivitis, N., Karlsson, H., Komppula, M., Laj, P., Li, S.-M., Lunder, C., Marinoni, A., Martins dos Santos, S., Moerman, M., Nowak, A., Ogren, J. A., Petzold, A., Pichon, J. M., Rodriquez, S., Sharma, S., Sheridan, P. J., Teinilä, K., Tuch, T., Viana, M., Virkkula, A., Weingartner, E., Wilhelm, R., and Wang, Y. Q.: Characterization and intercomparison of aerosol absorption photometers: result of two intercomparison workshops, Atmos. Meas. Tech., 4, 245–268, https://doi.org/10.5194/amt-4-245-2011, 2011a.

Müller, T., Laborde, M., Kassell, G., and Wiedensohler, A.: Design and performance of a three-wavelength LED-based total scatter and backscatter integrating nephelometer, Atmos. Meas. Tech., 4, 1291–1303, doi:10.5194/amt-4-1291-2011, 2011b.

Müller, T., Nowak, A., Wiedensohler, A., Sheridan, P., Laborde, M., Covert, David S., Marinoni, A., Imre, K., Henzing, B., Roger, J-C., dos Santos, S. M., Wilhelm, R., Wang, Y-Q., and de Leeuw, G.: Angular Illumination and Truncation of Three Different Integrating Nephelometers:

Implications for Empirical, Size-Based Corrections, Aerosol Sci. Tech., 43,581-586, doi:10.1080/02786820902798484, 2009.

Nam, J., Kim, S. W., Park, R. J., Park, J. S., and Park, S. S.: Changes in column aerosol optical depth and ground-level particulate matter concentration over East Asia, Air Quality, Atmosphere and Health, 11(1), 49–60, https://doi.org/10.1007/s11869-017-0517-5, 2018.

Nessler, R., Weingartner, E., and Baltensperger, U.: Effect of humidity on aerosol light absorption and its implications for extinction and the single scattering albedo illustrated for a site in the lower free troposphere, J. Aerosol Sci., 36, 958–972. https://doi.org/DOI: 10.1016/j.jaerosci.2004.11.012, 2005.

Ningombam, S. S., Larson, E. J. L., Dumka, U. C., Estellés, V., Campanelli, M., and Steve, C.: Long-term (1995–2018) aerosol optical depth derived using ground based AERONET and SKYNET measurements from aerosol aged-background sites, Atmos. Poll. Res., 10(2), 608–620, https://doi.org/10.1016/j.apr.2018.10.008, 2019.

Ogren, J. A.: Comment on "Calibration and Intercomparison of Filter-Based Measurements of Visible Light Absorption by Aerosols", Aerosol Sci. Tech., 44, 589–591, doi:10.1080/02786826.2010.482111, 2010.

Ogren, J.A., Wendell, J., Andrews, E., and Sheridan, P.: Continuous light absorption photometer for long-term studies, Atmos. Meas. Tech., 10, 4805-4818, https://doi.org/10.5194/amt-10-4805-2017, 2017.

Pandolfi, M., Alastuey, A., Pérez, N., Reche, C., Castro, I., Shatalov, V., and Querol, X.: Trends analysis of PM source contributions and chemical tracers in NE Spain during 2004–2014: a multi-exponential approach, Atmos. Chem. Phys., 16, 11787–11805, https://doi.org/10.5194/acp-16-11787-2016, 2016.

Pandolfi, M., Alados-Arboledas, L., Alastuey, A., Andrade, M., Angelov, C., Artiñano, B., Backman, J., Baltensperger, U., Bonasoni, P., Bukowiecki, N., Collaud Coen, M., Conil, S., Coz, E., Crenn, V., Dudoitis, V., Ealo, M., Eleftheriadis, K., Favez, O., Fetfatzis, P., Fiebig, M., Flentje, H., Ginot, P., Gysel, M., Henzing, B., Hoffer, A., Holubova Smejkalova, A., Kalapov, I., Kalivitis, N., Kouvarakis, G., Kristensson, A., Kulmala, M., Lihavainen, H., Lunder, C., Luoma, K., Lyamani, H., Marinoni, A., Mihalopoulos, N., Moerman, M., Nicolas, J., O'Dowd, C., Petäjä, T., Petit, J.-E., Pichon, J. M., Prokopciuk, N., Putaud, J.-P., Rodríguez, S., Sciare, J., Sellegri, K., Swietlicki, E., Titos, G., Tuch, T., Tunved, P., Ulevicius, V., Vaishya, A., Vana, M., Virkkula, A., Vratolis, S., Weingartner, E., Wiedensohler, A., and Laj, P.: A European aerosol phenomenology – 6: scattering properties of atmospheric aerosol particles from 28 ACTRIS sites, Atmos. Chem. Phys., 18, 7877–7911, https://doi.org/10.5194/acp-18-7877-2018, 2018.

Peterson, T.C., Easterling, D.R., Karl, T.R., Groisman, P., Nicholls, N., Plummer, N., Torok, S., Auer, I., Boehm, R., Gullett, D., Vincent, L., Heino, R., Tuomenvirta, H., Mestre, O., Szentimrey, T., Salinger, J., Forland, E., Hanssen-Bauer, I., Alexandersson, H., Jones, P., and Parker, D.: Homogeneity Adjustments of in Situ Atmospheric Climate Data: a Review, International Journal of Climatology, 18, 1493–1517, 1998.

Prenni, A. J., Hand, J. L., Malm, W. C., Copeland, S., Luo, G., Yu, F., Taylor, N., Russell, L.M. and Schichtel, B. A.: An examination of the algorithm for estimating light extinction from IMPROVE particle speciation data, Atmos. Environ., 214, https://doi.org/10.1016/j.atmosenv.2019.116880, 2019.

Ridley, D. A., Heald, C. L., and Prospero, J. M.: What controls the recent changes in African mineral dust aerosol across the Atlantic?, Atmos. Chem. Phys., 14, 5735–5747, https://doi.org/10.5194/acp-14-5735-2014, 2014.

Rose, C., Sellegri, K., Freney, E., Dupuy, R., Colomb, A., Pichon, J.-M., Ribeiro, M., Bourianne, T., Burnet, F., and Schwarzenboeck, A.: Airborne measurements of new particle formation in

the free troposphere above the Mediterranean Sea during the HYMEX campaign, Atmos. Chem. Phys., 15, 10203–10218, https://doi.org/10.5194/acp-15-10203-2015, 2015.

Schmeisser, L., Andrews, E., Ogren, J. A., Sheridan, P., Jefferson, A., Sharma, S., Kim, J.E., Sherman, J.P., Sorribas, M., Kalapov, I., Arsov, T., Angelov, C., Mayol-Bracero, O., Labuschagne, C., Kim, S.-W., Hoffer, A., Lin, N.-H., Chia, H.-P., Bergin, M., Sun, J., Liu, P., and Wu, H.: Classifying aerosol type using in situ surface spectral aerosol optical properties, Atmos. Chem. Phys., 17(19), 12097–12120. https://doi.org/10.5194/acp-17-12097-2017, 2017.

Schmeisser, L., Backman, J., Ogren, J. A., Andrews, E., Asmi, E., Starkweather, S., Uttal, T., Fiebig, M., Sharma, S., Eleftheriadis, K., Vratolis, S., Bergin, M., Tunved, P., and Jefferson, A.: Seasonality of aerosol optical properties in the Arctic, Atmos. Chem. Phys., 18, 11599–11622, https://doi.org/10.5194/acp-18-11599-2018, 2018.

Schuster, G. L., Dubovik, O., and Holben, B.N.: Ångström exponent and bimodal aerosol size distributions, J. Geophys. Res.,111, D07207, doi:10.1029/2005JD006328, 2006.

Sheridan, P., Andrews, E., Schmeisser, L., Vasel, B., and Ogren, J.: Aerosol measurements at South Pole: Climatology and impact of local contamination, Aerosol and Air Quality Research, 16(3), 855–872. https://doi.org/10.4209/aaqr.2015.05.0358, 2016.

Sherman, J. P., Sheridan, P. J., Ogren, J. A., Andrews, E., Hageman, D., Schmeisser, L., Jefferson, A., and Sharma, S.: A multi-year study of lower tropospheric aerosol variability and systematic relationships from four North American regions, Atmos. Chem. Phys., 15, 12487–12517, https://doi.org/10.5194/acp-15-12487-2015, 2015.

Singh, V., Ravindra, K., Sahu, L., and Sokhi, R.: Trends of atmospheric black carbon concentration over United Kingdom, Atmos. Environ., 178, 148–157. https://doi.org/10.1016/j.atmosenv.2018.01.030, 2018.

Sirois, A.: A brief and biased overview of time-series analysis of how to find that evasive trend, WMO/EMEP Workshop on Advanced Statistical Methods and Their Application to Air Quality Data Sets, Annex E., Global Atmosphere Watch No. 133, TD- No. 956, World Meteorological Organization, Geneva, Switzerland, 1998.

Sogacheva, L., Popp, T., Sayer, A. M., Dubovik, O., Garay, M. J., Heckel, A., Hsu, N. C., Jethva, H., Kahn, R. A., Kolmonen, P., Kosmale, M., de Leeuw, G., Levy, R. C., Litvinov, P., Lyapustin, A., North, P., and Torres, O.: Merging regional and global AOD records from 15 available satellite products, Atmos. Chem. Phys. Discuss., https://doi.org/10.5194/acp-2019-446, in review, 2019.

Tørseth, K., Aas, W., Breivik, K., Fjæraa, A. M., Fiebig, M., Hjellbrekke, A. G., Lund Myhre, C., Solberg, S., and Yttri, K. E.: Introduction to the European Monitoring and Evaluation Programme (EMEP) and observed atmospheric composition change during 1972–2009, Atmos. Chem. Phys., 12, 5447–5481, doi:10.5194/acp-12-5447-2012, 2012.

Vestreng, V., Myhre, G., Fagerli, H., Reis, S., and Tarrasón, L.: Twenty-five years of continuous sulphur dioxide emission reduction in Europe, Atmos. Chem. Phys., 7, 3663–3681, https://doi.org/10.5194/acp-7-3663-2007, 2007.

Virkkula, A., Ahlquist, N. C., Covert, D. S., Arnott, W. P., Sheridan, P. J., Quinn, P. K., and Coffman, D. J.: Modification, calibration and a field test of an instrument for measuring light absorption by particles, Aerosol Sci. Tech. 39(1), 68–83, https://doi.org/10.1080/027868290901963, 2005.

Virkkula, A.: Correction of the Calibration of the 3-wavelength Particle Soot Absorption Photometer (3λ PSAP), Aerosol Sci. Tech., 44:8, 706-712, DOI:10.1080/02786826.2010.482110, 2010.

Von Storch, H.: Misuses of statistical analysis in climate research. In: Analysis of Climate Variability: Applications of Statistical Techniques (ed. by H. von Storch & A. Navara), 11–26. Springer-Verlag, Berlin, Germany, 1995.

Wang, R., Andrews, E., Balkanski, Y., Boucher, O., Myhre, G., Samset, B.H., Schulz, M., Schuster, G., Valari, M., and Tao, S., Representativeness error in the ground-level observation networks for black carbon radiation absorption, Geophys. Res. Lett., doi:10.1002/2017GL076817, 2018.

Wang, W., Chen, Y., Becker, S., and Liu, B.: Linear trend detection in serially dependent hydrometeorological data based on a variance correction Spearman rho method, Water, 7(12), 7045–7065. https://doi.org/10.3390/w7126673, 2015.

Wang, X. L. and Swail, V. R: Changes of extreme wave heights in Northern Hemisphere oceans and related atmospheric circulation regimes, J. Climate, 14, 2204–2221, https://doi.org/10.1175/1520-0442(2001)014, 2001.

Weatherhead, E. C., Reinsel, G. C., Tiao, G. C., Jackman, C. H., Bishop, L., Hollandsworth, F. S. M., DeLuisi, J., Keller, T., Oltmans, S. J., Flemming, E. L.,Wuebbles, D. J., Kerr, J. B., Miller, A. J., Herman, J., McPeters, R., Nagatani, R. M., and Frederick, J. E.: Detecting the recovery of total column ozone, J. Geophys. Res., 105, 22201–22210, 2000.

White, W. H., Trzepla, K., Hyslop, N. P., and Schichtel, B. A.: A critical review of filter transmittance measurements for aerosol light absorption, and de novo calibration for a decade of monitoring on PTFE membranes, Aerosol Sci. Tech., 50(9), 984–1002, https://doi.org/10.1080/02786826.2016.1211615, 2016.

WMO/GAW aerosol measurement procedures, guidelines, and recommendations. 2nd ed. World Meteorological Organization GAW Rep. 227, 93 pp., https://library.wmo.int/opac/doc_num, 2016.

Yue, S., Pilon, P., Phinney, B., and Cavadias, G.: The influence of autocorrelation on the ability to detect trend in hydrological series, Hydrological Processes, 16(9), 1807–1829. https://doi.org/10.1002/hyp.1095, 2002.

Yoon, J., Pozzer, A., Chang, D.Y., Lelieveld, J., Kim, J., Kim, M., Lee, Y.G., Koo, J-H., Lee, J., and Moon, K.J., Trend estimates of AERONET-observed and model-simulated AOTs between 1993 and 2013, Atmos. Environ., 125, 33–47, http://dx.doi.org/10.1016/j.atmosenv.2015.10.058, 2016.

Zhang, X. and Zwiers, F. W.: Comment on "Applicability of prewhitening to eliminate the influence of serial correlation on the Mann-Kendall test" by Sheng Yue and Chun Yuan Wang, Water Resour. Res., 40, W03805, doi:10.1029/2003WR002073, 2004.

Zhang, X., Zwiers, F. W., and Li, G.: Monte Carlo experiments on the detection of trends in extreme values, J. Climate, 17(10), 1945–1952, https://doi.org/10.1175/1520-0442(2004)017, 2004.

Zhao, A., Bollasina, M. A., Crippa, M., and Stevenson, D. S.: Significant climate impacts of aerosol changes driven by growth in energy use and advances in emissions control technology, Atmos. Chem. Phys. Discuss., https://doi.org/10.5194/acp-2019-616, in review, 2019.

Zieger, P., Fierz-Schmidhauser, R., Weingartner, E., and Baltensperger, U.: Effects of relative humidity on aerosol light scattering: results from different European sites, Atmos. Chem. Phys., 13, 10609–10631, https://doi.org/10.5194/acp-13-10609-2013, 2013.

Atmospheric Chemistry and Physics Discussions — Open Access EGU

Tables

Table 1: List of observatories included in this study, arranged alphabetically by GAW acronyms, including their names, countries, coordinates and elevation, site environmental characteristic (geographical category and footprint), size cut, type of nephelometer and absorption filter photometer deployed, time period used, and nephelometer RH percentiles.

GAW code	Station Name	Country	GPS coordinates	Site Characteristics[1]	Size cut[2]	σ_{sp} Period[3]	σ_{ap} Period[4]	Sample RH 5th;50th;95th percentile
ACA	Acadia NP[5]	US	44.38°N, 68.26°W, 122 m	Coast, RB	-	O, 1994-2018	--	46;75;98
ALT	Alert	CA	82.50°N, 62.34°W, 210 m	P, P	PM10 & PM1	T, 2005-2017	P, 2005-2014 / C, 2014-2017	0;4;23
AMY	Anmyeon-do	KR	36.54°N, 126.33°E, 46 m	Coast, RB	PM10	T, 2008-2018	AE16, 2008-2009 / AE31, 2010-2018	8;26;66
APP	Appalachian	US	36.21°N, 81.69°W, 1076 m	Con, RB	PM10 & PM1	T, 2010-2018	P, 2010-2016 / C, 2016-2018	0;17;41
BBE	Big Bend NP	US	29.30°N, 103.18°W, 1052 m	Con, DE	-	O, 1998-2015	--	14;41;78
BEO	Moussala	BG	42.18°N, 23.59°E, 2925 m	Mt, Mix	TSP	T, 2008-2017	--	4;15;26
BIR	Birkenes	NO	58.38°N, 8.25°E, 220 m	Con, F	PM10	T, 2010-2018	P, 2010-2018	11;21;38
BND	Bondville	US	40.05°N, 88.37°W, 213 m	Con, RB	PM10 & PM1	T, 1995-2018	P, 1998-2012 / C, 2012-2018	5;22;47
BRW	Barrow	US	71.32°N, 156.61°W, 11 m	Polar, Coast, P	TSP- PM10 &PM1	R, 1978-1997 / T, 1997-2018	P, 1998-2014 / C, 2014-2018	0;7;26
CGO	Cape Grim	AU	40.68°S, 144.69°E, 94 m	Coast, RB	PM10 & PM1	E, 2006-2018	M, 2008-2018	0;9;23
CMN	Monte Cimone	IT	44.17°N, 10.68°E, 2165 m	Mt, Mix	TSP	--	M, 2008-2018	14;34;57
CPR	Cape San Juan	PR	18.38°N, 65.62°W, 65 m	Coast, F	PM1 & PM10	T, 2005-2016	P, 2007-2014 / C, 2014-2016	31;48;70
CPT	Cape point	ZA	34.35°S, 18.49°E, 230 m	Coast, Mix	PM1 & PM10	T, 2006-2014	P, 2006-2014	25;36;51
CRG	Columbia River George	US	45.66°N, 121.00°W, 178 m	Con, RB	-	O, 1994-2004	--	35;63;92
EGB	Egbert	CA	44.23°N, 79.78°W, 255 m	Con, RB	PM10	T, 2010-2018	P, 2010-2018	6;23;60
FKL	Finokalia	GR	35.34°N, 25.67°E, 150 m	Coast, RB	TSP-PM10 PM10 PM10	--	AE21, 2004-2010 / AE31, 2011-2014 / AE33, 2015-2018	29;64;90
GBN	Great Basin NP	US	39.01°N, 114.22°W, 2065 m	Mt, DE	-	O, 2008-2018	--	14;41;80
GLR	Glacier NP	US	48.51°N, 114.00°W, 976 m	Con, F	-	O, 2008-2018	--	48;78;95
GSM	Great Smoky Mountain NP	US	35.63°N, 83.94°W, 810 m	Con, F	-	O, 1994-2018	--	40;73;98
GSN	Gosan	KR	33.28°N, 126.17°E, 72 m	Coast, RB	TSP-PM10 & PM1	T, 2008-2015	AE31, 2008-2015	14;30;64

Code	Station	Country	Location	Class	Size	Meas	Instrument	Values
HGC	Grand Canyon NP	US	35.97°N, 111.98°W, 2267 m	Con, F	-	O, 1998-2018	--	18;45;91
HPB	Hohenpeissenberg	DE	47.80°N, 11.01°E, 985 m	Mt, RB	TSP-PM10	T, 2006-2017	M, 2004-2017	9;23;44
IPR	Ispra	IT	45.80°N, 8.63°E, 209 m	Con, U	PM10	T, 2004-2017	AE31, 2004-2017	6;24;56
IZO	Izana	ES	28.31°N, 16.50°W, 2373 m	Mt, Mix	PM10	T, 2009-2018	M, 2007-2018	5;15;33
JFJ	Jungfraujoch	CH	46.55°N, 7.99°E, 3580 m	Mt, Mix	TSP	T, 1996-2018	AE31, 2002-2018	0;7;16
KPS	K-Pustza	HU	46.97°N, 19.58°E, 125 m	Con, RB	PM1-PM10	T, 2008-2017	P, 2008-2012; C, 2012-2018	11;24;44
LLN	Lulin	TW	23.47°N, 120.87°E, 2862 m	Mt, F, Mix	PM10 & PM1	T, 2009-2018	P, 2009-2011; C, 2012-2018	5;16;44
MCN	Mammoth Caves NP	US	37.13°N, 86.15°W, 235 m	Con, RB	-	O, 1993-2018	--	48;78;99
MEL	Melpitz	DE	51.53°N, 12.93°E, 86 m	Con, U	PM10	T, 2007-2017	M, 2007-2017	7;20;34
MLO	Mauna Loa	US	19.54°N, 155.58°W, 3397 m	Mt, Mix	TSP-PM10 & PM1	T, 2000-2018	MRI, 1988-1999; P, 2000-2013; C, 2013-2018	0;6;18
MRN	Mount Rainier NP	US	46.76°N, 122.12°W, 439 m	Con, F	-	O, 1993-2018	--	68;92;100
MSY	Montseny	ES	41.78°N, 2.36°E, 700 m	Mt, RB	PM10	E, 2010-2018	M, 2009-2018	15;26;43
MUK	Mukteshwar	IN	29.44°N, 79.62°E, 2180 m	Mt, Mix	PM2.5-PM10	E, 2006-2013	AE31, 2006-2015	2;7;15
MZW	Mt. Zirkel Wilderness	US	40.54°N, 106.68°W, 3243 m	Mt, F	-	O, 1994-2008	--	28;65;92
NCC	National Capitol Central	US	38.90°N, 77.04°W, 514 m	Con, U	-	O, 2004-2015	--	38;63;90
NMY	Neumayer	DE	70.67°S, 8.27°W, 42 m	Polar, Coast, Mix	PM10	T, 2009-2018	M, 2007-2018	0;2;10
PAL	Pallas	FI	67.97°N, 24.12°E, 560 m	Polar, Pristine	PM5-PM2.5-PM10	T, 2000-2018	M, 2008-2018	4;12;32
PAY	Payerne	CH	46.81°N, 6.94°E, 490 m	Con, RB	PM2.5	--	AE31, 2009-2018	??
PUY	Puy de Dôme	FR	45.77°N, 2.97°E, 1465 m	Mt, Mix	TSP	T, 2009-2018	M, 2009-2017	10;26;49
RMN	Rocky Mountain NP	US	40.28°N, 105.55°W, 2760 m	Mt, RB	-	O, 2008-2018	--	21;48;88
SCN	Sycamore Canyon	US	35.14°N, 111.97°W, 2046 m	Con, F	-	O, 1999-2009	--	17;50;97
SGP	Southern Great Plains	US	36.60°N, 97.50°W, 318 m	Con, RB	PM10 & PM1	T, 1997-2017	P, 1997-2017	5;25;53
SHN	Shenandoah	US	38.52°N, 78.44°W, 1074 m	Con, F	-	O, 1997-2018	--	41;78;100
SMR	Hyytiala	FI	61.85°N, 24.29°E, 181 m	Con, F	TSP-PM10	T, 2007-2017	AE31, 2007-2017	4;14;47
SPO	South Pole	US	90.00°S, 24.80°W, 2841 m	Polar, P	TSP	T, 1979-2018	--	0;0;0
SUM	Summit	DK	72.58°N, 38.48°W, 3238 m	Polar, P	TSP	--	AE16, 2006-2016; C, 2016-2018	0;0;5
THD	Trinidad Head	US	41.05°N, 124.15°W, 107 m	Coast, RB	PM10 & PM1	T, 2003-2016	P, 2003-2013; C, 2013-2016	16;27;38
TIK	Tiksi	RU	71.59°N, 128.92°E, 8 m	Polar, Coast, RG	PM10	--	AE31, 2010-2018	??
UGR	Granada	ES	37.16°N, 3.61°W, 680 m	Con, U	TSP	T, 2006-2018	M, 2006-2018	14;29;46
WLG	Mount Waliguan	CN	36.29°N, 100.90°E, 3810 m	Mt, Mix	PM10 & PM1	T, 2008-2018	P, 2008-2018	0;8;23
ZEP	Zeppelin Mountain	NO	78.91°N, 11.89°E, 475 m	Polar, Mt, P	PM10	T, 2005-2016	P, 2005-2018 AE31	0;7;17
ZSF	Zugspitze-Schneefernerhaus	DE	47.42°N, 10.58°E, 2671 m	Mt, Mix	TSP & PM10	--	M, 2009-2018	4;13;24

¹ Geographical category: Mountain=**Mt**, Polar=**P**, Continental=**Con**, Coastal =**Coast**

Footprint: Rural background=**RB**, Forest=**F**, Desert=**DE**, (Sub-)Urban=**U**, Pristine= **P** Mixed: **Mix**

² the mention of two size cuts separated by " - " corresponds to a modification of inlet during the tim series, whereas the "&" corresponds to measurements at two size cuts.

*³ T=TSI nephelometer, O=Optec nephelometer, R=Radiance Research nephelometer;E3=Ecotech nephelometer Aurora 3000, E4=Ecotech nephelometer Aurora 4000

⁴ AE16(C_ref =1.8)/AE22 (C_ref =??)/AE31 (C_ref =3.5)/AE33 (C_ref =3.5)/Aethalometer , P1=1-wavelength or P3=3-wavelength PSAP, M=MAAP, C=NOAA CLAP , ET=ES95L Thermo 5012==M

Atmospheric Chemistry and Physics Discussions — Open Access

Table 2: MK trends for all parameters in units/y for the last 10 y, 15 y and 20 y of measurements ending in 2016-2018. The ss trends are given in bold. Results in %/y are given in Table S1.

Station	σ_{sp} 10 y	15 y	20 y	σ_{bsp} 10 y	15 y	20 y	σ_{ap} 10 y	15 y	20 y	ω_o 10 y	15 y	20 y	b 10 y	15 y	20 y	$\mathring{a}_{sp}$ 10 y	15 y	20 y	$\mathring{a}_{ap}$ 10 y	15 y
Africa																				
IZO	-0.106			-0.009			**-0.008**			**0.000**			**0.000**			0.001				
Asia																				
AMY	**-0.741**			-0.069			-0.007			**-0.001**			0.000			**0.012**	**0.012**			
LLN	-0.044			-0.005			**-0.044**			**0.003**			**0.001**			**0.018**			0.005	
WLG	-0.348			0.019			**-0.051**			**0.000**			**0.002**			0.012			**0.024**	
Europe																				
BEO	-0.032			0.023			-0.014						-0.001			**-0.016**				
BIR	**-0.092**			**-0.012**						0.001			0.000			**-0.013**				
CMN							-0.010													
FKL							0.004	-0.002												
HPB	**-0.280**			-0.029			-0.063			**0.001**			0.000							
HYY	**-0.193**			-0.022			-0.038			**0.002**			**0.001**			**0.011**	**0.011**		**-0.004**	
IPR	**-2.454**			-0.317			-0.124			**-0.006**			**0.001**			**-0.007**			0.002	
JFJ	**-0.092**	**0.062**	**-0.032**	-0.007	-0.006	-0.004	-0.011	-0.004		-0.002	-0.001					**-0.030**	**-0.008**	**0.004**	**-0.007**	**-0.006**
KPS	-0.033			-0.004			-0.019			0.001			0.000			-0.002				
MPZ	**-1.043**			-0.171			-0.133			0.000			0.000			0.008				
MSY	**-1.155**			-0.095			-0.027			-0.003			**0.003**			0.006				
PAL	**0.064**	0.013		0.012	0.003		-0.004			**0.003**			0.000	0.000		0.005	-0.002			
PAY							-0.201													
PUY	-0.147			-0.015			-0.017			0.002			**0.002**			-0.022				
UGR	0.330			0.062			-0.031			**0.001**			**0.001**			0.007				
ZSF							-0.036													
North America																				
ACA	**-0.606**	**0.313**	**-0.284**	-0.074			-0.092			**0.001**			**0.002**							
APP	**-0.627**															**-0.007**			0.000	
BND	**-0.787**	**0.526**	**-0.413**	-0.107	-0.071	-0.056	-0.060	-0.065	-0.029	0.000	0.000	0.000	**0.000**	**0.000**	**0.000**	**0.008**	0.001	0.003	
CPR	**0.394**			0.037			-0.009			**0.001**			**0.000**			**-0.018**			**0.099**	

EGB	0.063			0.036			0.029			0.000			0.003	-0.027	-0.023	
GBN	-0.349															
GLR	0.435															
HGC	-0.152	-0.158	-0.061													
MCN	-1.454	-1.161	-0.821													
MRN	-0.041	-0.104	-0.208													
RMN	-0.074															
SGP	-0.220	-0.299	-0.280	-0.028	-0.045	-0.031	-0.015			-0.001			0.000	-0.008	-0.007	0.016
SHN	-0.784	-0.673	-0.539													
THD	-0.634			-0.070			-0.007			0.000			0.013		0.000	
South Pacific																
CGO	0.124						0.000		0.000	0.000			0.000			
MLO	-0.012	0.000	0.005	-0.001	0.001		-0.002	0.001	-0.002	0.002	0.005		0.010	-0.019	-0.012	0.084
Polar regions																
ALT	-0.019			-0.003			0.002		0.001	0.001			0.002	0.017		0.008
BRW	-0.209	-0.066	-0.039	-0.016	-0.004	-0.003	-0.007	0.000	0.000	0.002	0.001	0.000	0.014	0.005	-0.002	-0.001
NMY	0.008			-0.001			0.000		0.000	0.000			-0.001	-0.005		
SPO	0.006	0.000	0.004	0.003	0.000	0.000	0.000	0.000		0.006			-0.024	-0.024	-0.031	
SUM							0.000		0.000	0.000						
TIK				-0.007			-0.007								-0.003	
ZEP	0.050			0.007			-0.001		0.001	0.001			0.001	-0.018	-0.002	0.004

Table 3: Number of trends analyzed for each parameters, of ss cases for each trend analysis methods, of trends with similar significance in MK, GLS/day and LMS/log, of trends with similar statistical significance for all the five methods, of trends with at least GLS/day or LMS/log ss similar to MK, of trends with none agreement between these two methods and MK ss.

Number of	σ_{sp}	σ_{bsp}	σ_{ap}	ω_0	b	$\mathring{a}_{sp}$	$\mathring{a}_{ap}$
Time series	37	28	33	27	26	27	14
ss MK	23	17	21	19	19	18	8
ss GLS/day	27	19	24	22	20	21	7
ss GLS/month	22	16	21	12	17	12	9
ss LMS/log	25	18	17	12	17	14	5
ss LMS/lin	22	17	21	12	17	13	7
MK, GLS/day and LMS/log identical	29	24	22	12	17	19	9
all 5 methods identical	27	23	20	10	15	16	7
MK+ GLS/day or LMS/log identical	4	3	7	12	7	7	2
MK different from GLS/day or LMS/log	4	1	4	3	2	1	3

Table 4: Overview of the aerosol optical properties decadal MK trends ending between 2016-2018 for all the stations and per continent/region of the world.

Regions (nb stations/nb ss trends)	Mean trend for all stations [%/y] (std)	Mean ss trend [%/y] (std)
Scattering coefficient		
all (37/23)	-2.11 (3.27)	-2.85 (3.77)
Africa (1/0)	-4.6	
Asia (3/0)	-1.3 (0.44)	
Europe (12/8)	-2.92 (3.42)	-4.03 (3.56)
N.-America (14/10)	-2.66 (2.95)	-3.66 (2.79)
Pacific (2/1)	0.96 (3.7)	3.57
Polar regions (5/4)	0.15 (4.04)	-0.05 (4.63)
Backscattering coefficient		
all (28/17)	-0.91 (3.4)	-1.35 (4.13)
Africa (1/0)	-2.31	
Asia (3/0)	-0.45 (0.95)	
Europe (12/8)	-1.67 (3.46)	-2.9 (3.3)
N. America (6/6)	-1.32 (3.24)	-1.32 (3.24)
Pacific (1/0)	-0.57	
Polar regions (5/3)	1.34 (4.73)	2.7 (6.14)
Absorption coefficient		
all (33/21)	-2.94 (3.36)	-4.02 (3.45)
Africa (1/1)	-3.84	-3.84
Asia (3/2)	-3.31 (3.26)	-4.83 (2.73)
Europe (15/11)	-3.72 (3.41)	-4.45 (3.6)
N. America (6/2)	-1.85 (2.87)	-4.24 (1.58)
Pacific (2/1)	-1.4 (3.31)	-3.74
Polar regions (6/4)	-2.25 (4.46)	-2.47 (5.34)
Single scattering albedo		
all (27/19)	0.02 (0.26)	0.01 (0.31)
Africa (1/0)	-0.02	
Asia (3/3)	0.12 (0.25)	0.12 (0.25)
Europe (11/8)	-0.03 (0.38)	-0.09 (0.44)
N. America (6/5)	-0.01 (0.11)	-0.01 (0.12)
Pacific (2/1)	0.13 (0.19)	0.27

Polar regions (4/2)	0.05 (0.07)	0.11 (0.01)
Backscattering fraction		
all (26/19)	0.99 (1.52)	1.41 (1.58)
Africa (1/1)	0.41	0.41
Asia (3/2)	1.32 (0.75)	1.75 (0.16)
Europe (10/6)	0.42 (1.1)	0.86 (1.26)
N. America (6/5)	0.79 (0.93)	0.91 (0.99)
Pacific (1/1)	3.79	3.79
Polar regions (5/4)	1.75 (2.58)	2.34 (2.56)
Scattering Ångström exponent		
all (27/18)	-0.14 (1.78)	-0.3 (2.06)
Africa (1/0)	0.15	
Asia (3/2)	1.41 (0.25)	1.28 (0.13)
Europe (11/7)	-0.23 (0.93)	-0.58 (0.99)
N. America (6/6)	-1.01 (2.99)	-1.01 (2.99)
Pacific (1/0)	0.86	
Polar regions (5/3)	-0.09 (1.98)	0.75 (2.17)
Absorption Ångström exponent		
all (14/8)	1.34 (2.59)	2.33 (3.14)
Asia (2/1)	1.42 (1.25)	2.3
Europe (3/2)	-0.32 (0.54)	-0.62 (0.16)
N. America (4/2)	2.31 (3.6)	4.62 (4.17)
Pacific (1/1)	6.66	6.66
Polar regions (4/2)	0.26 (0.7)	0.82 (0.37)

Figures

Figure 1: Map of stations with their GAW acronyms

Figure 2: Seasonal MK results for σ_{sp} trend for three stations with long time series: JFJ, RMN and MLO. The trends are plotted for the last 10 years period (2009-2018) as well as for all possible longer periods (15 y=2004-2018 to 30 y=1989-2018). The seasons correspond to meteorological seasons (MAM= March-April-May, JJA= June-July-August, SON=September-October-November and DJF= December-January-February). The dots correspond to the slope, large dots being ss at 95% confidence level whereas small dot are not ss trends. The cyan

triangles correspond to false positive trends (with type I error). Red squares correspond to annual trends where the seasonal results are homogeneous.
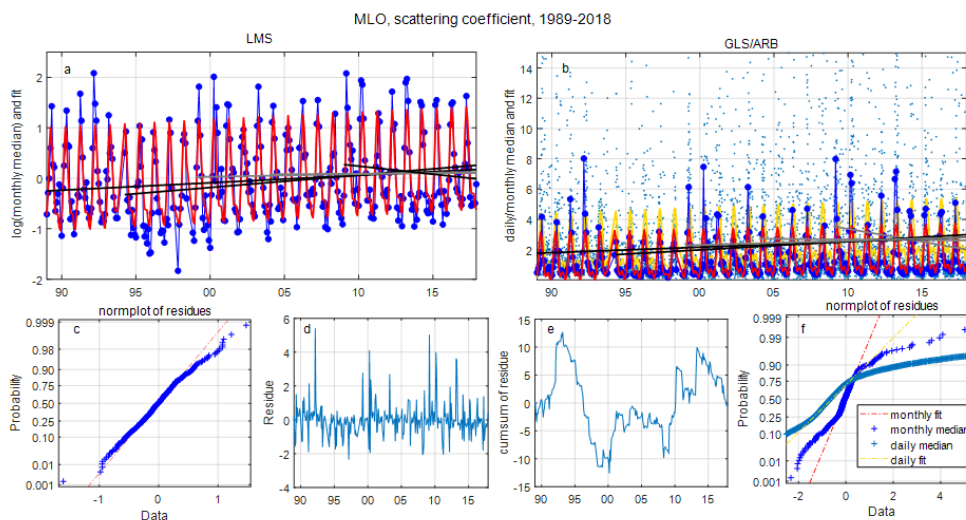
Figure 3: LMS and GLS/ARB results of MLO σ_{sp}: a) Logarithm of the monthly medians (blue circles), LMS fit (red) and the 10 y to 30 y slopes (ss slopes are plotted in black and not ss slopes in grey), b) daily medians (light blue dots) and their GLS/ARB fit (orange line), monthly medians (blue circles) and their GLS/ARB fit (red) and the 10 y to 30 y slopes, c) normplot of LMS residues, d) monthly medians of the GLS/ARB residues, e) cumulative summation of monthly median GLS/ARB residues and f) normplot of GLS/ARB residues for daily medians (light blue crosses and orange line) and monthly medians (blue crosses and red line).
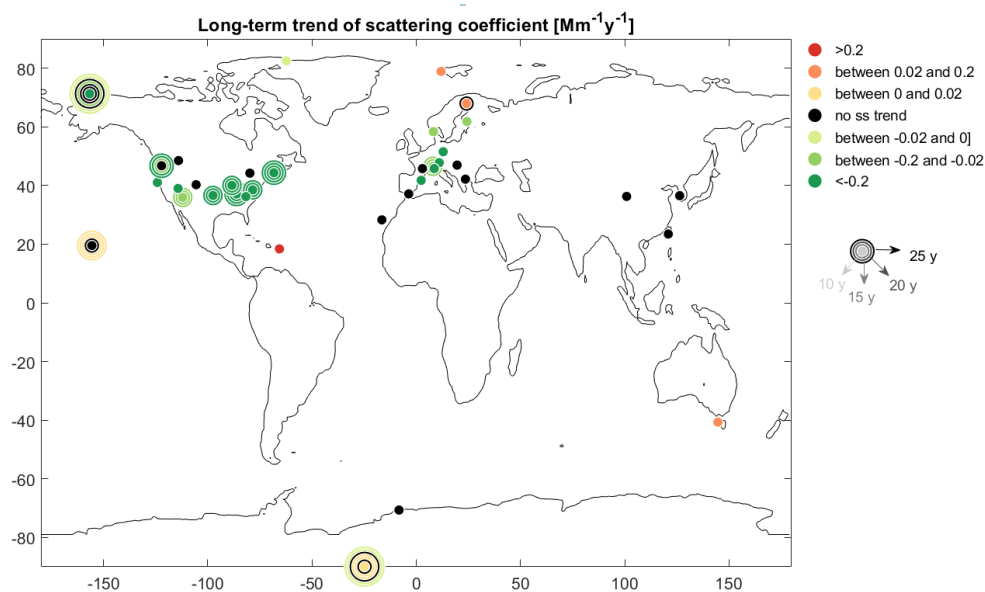
Figure 4: MK trends results for the scattering coefficient. Black symbols correspond to stations with no significant trends. Green and orange symbols correspond to ss negative and positive trends, respectively. The magnitude of the trends (slope) is given by the colors as stipulated in the legend. The size of the circles is proportional to the length of the data sets with the central dots representing the most recent 10 y trend ending in 2016, 2017 or 2018. If possible, trends for longer time periods were calculated and the larger circles denote the trends for 15 y to 40 y in 5 y increments.
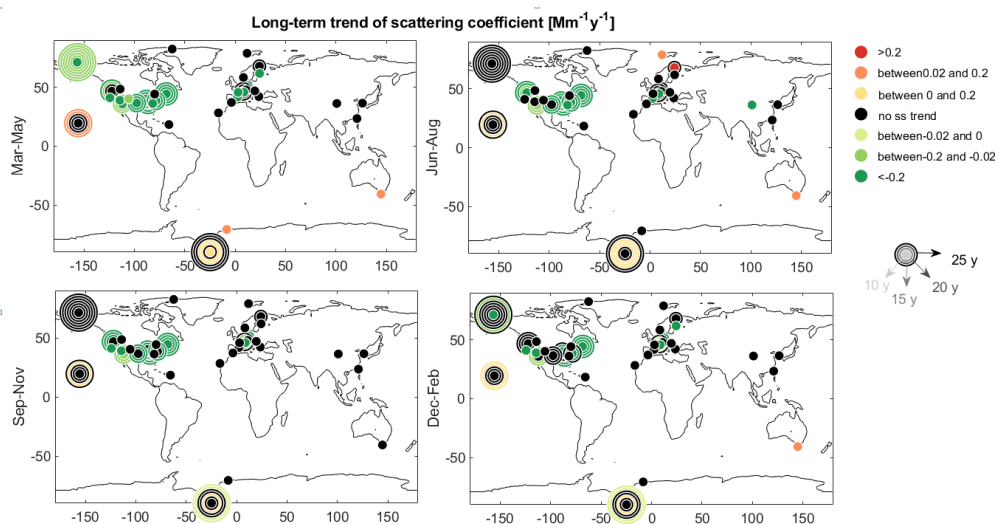
Figure 5: Seasonal results of the MK trend of the scattering coefficient. Other details same as Fig. 4.
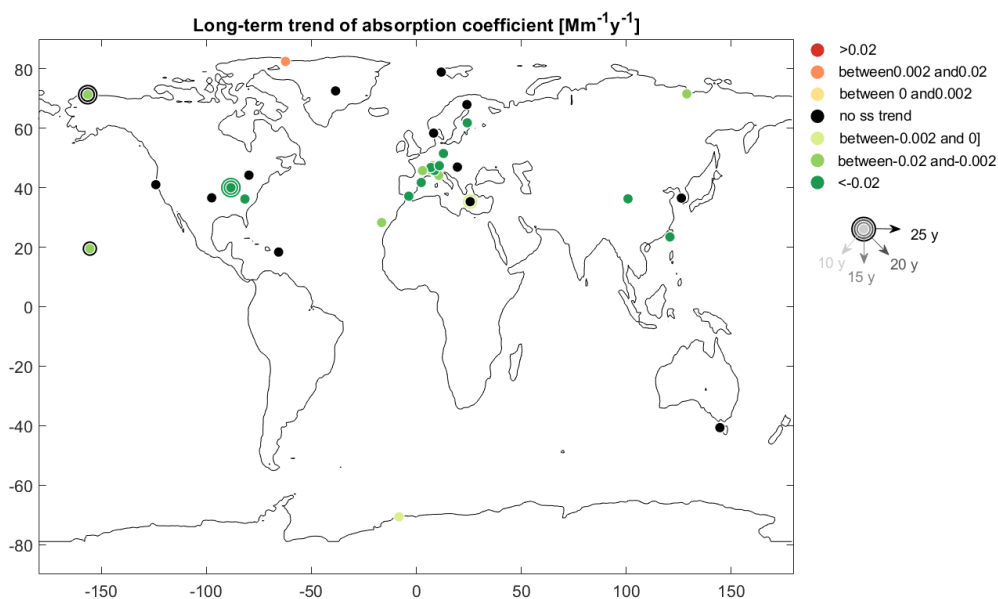
Figure 6: MK trends results for the absorption coefficient. Other details same as Fig. 4.
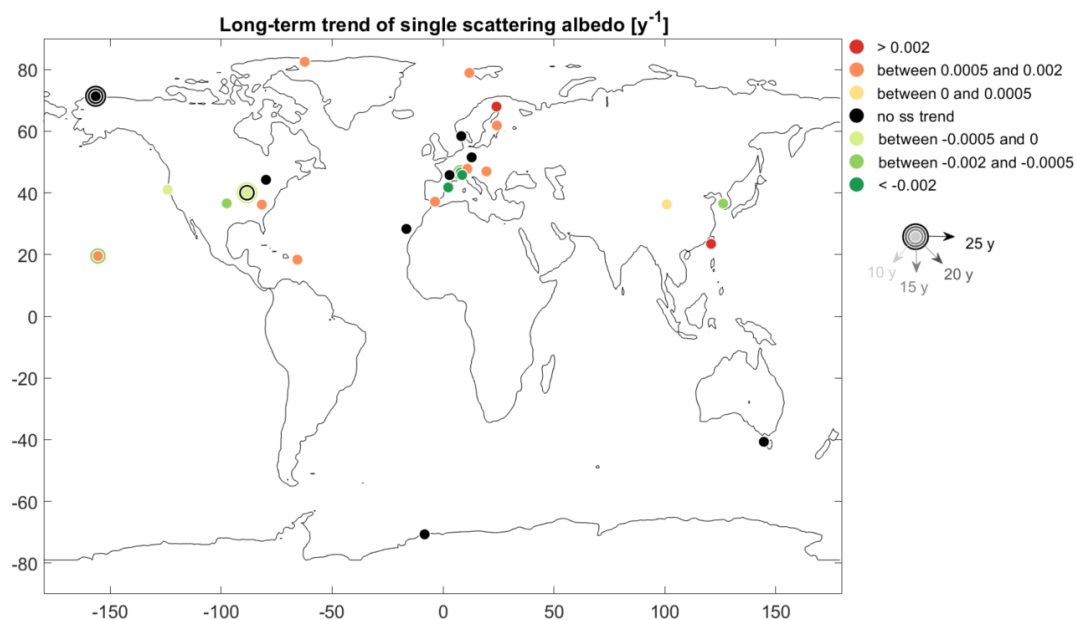
Figure 7: MK trend results for the single scattering albedo. Other details same as Fig. 4
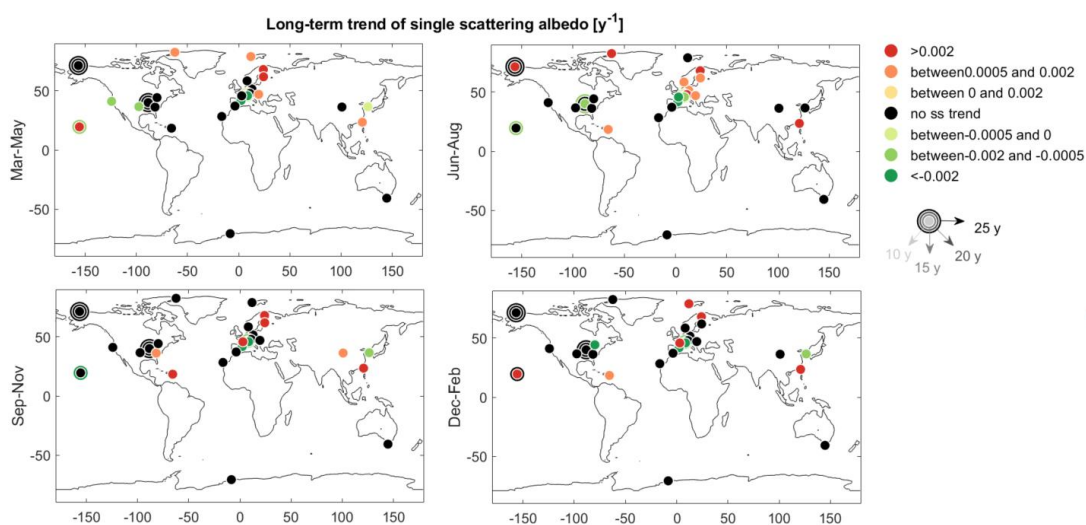
Figure 8: Seasonal results of the MK trend of the single scattering albedo. Other details same as Fig. 4.
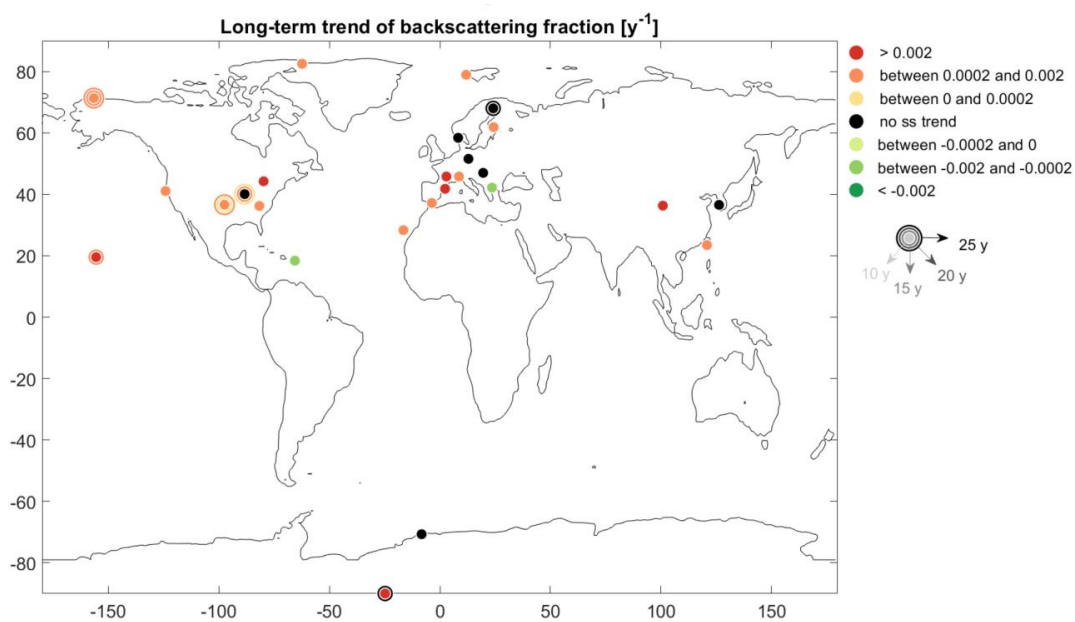
Figure 9: MK trends results for the backscattering fraction. Other details same as Fig. 4
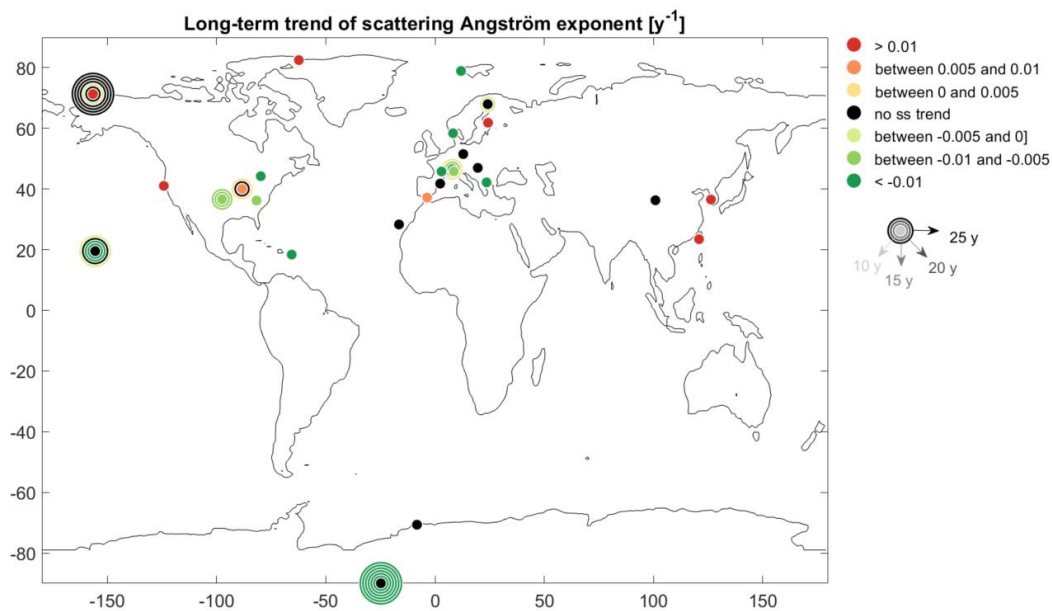
Figure 10: MK trend results for the scattering Ångström exponent. Other details same as Fig. 4.
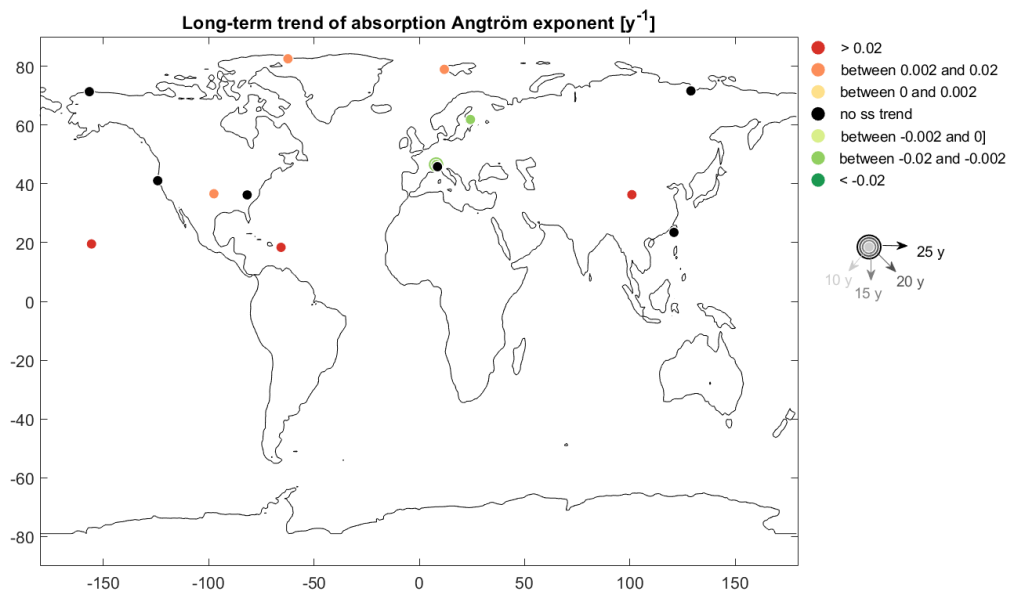
Figure 11: MK trends results for the absorption Ångström exponent. Other details same as Fig. 4.
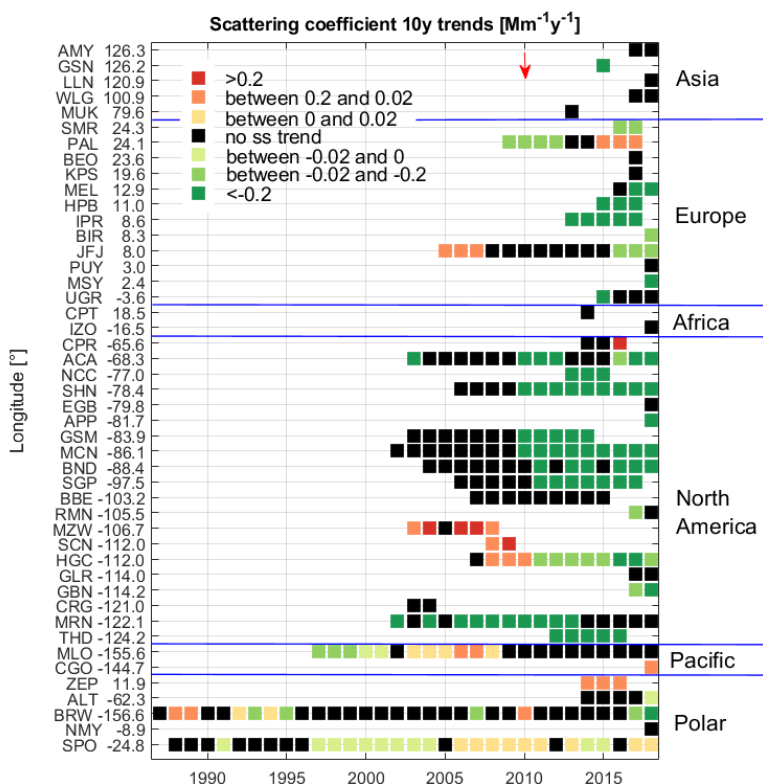
Figure 12: Time series of sequential 10 y σ_{sp} trends as a function of station longitude. Stations in the South Pacific and in polar regions were grouped for clarity. The red arrow indicates the end of the time periods covered in CC2013.
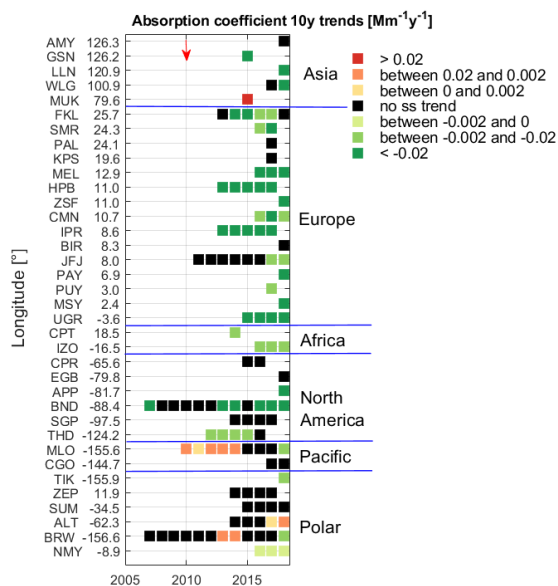
Figure 13: Time series of sequential 10 y σ_{ap} trends as a function of station longitude. The red arrow indicates the end of the time period covered in CC2013.
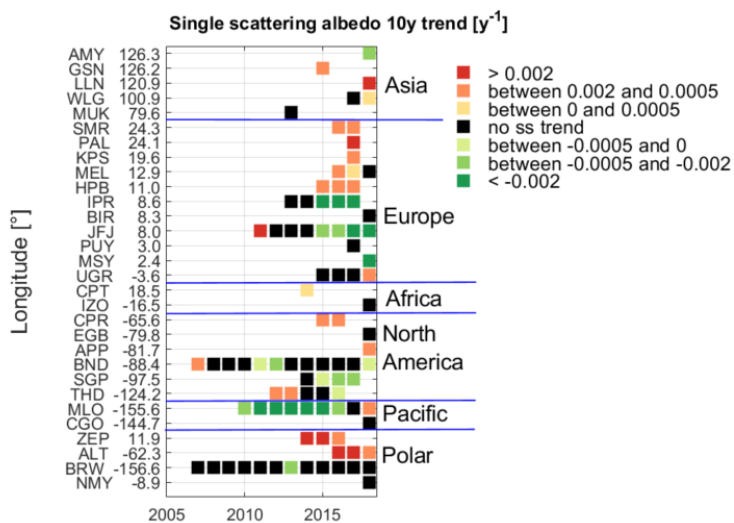
Fig 14: Time series of sequential 10 y ω_0 trends as a function of station longitude.
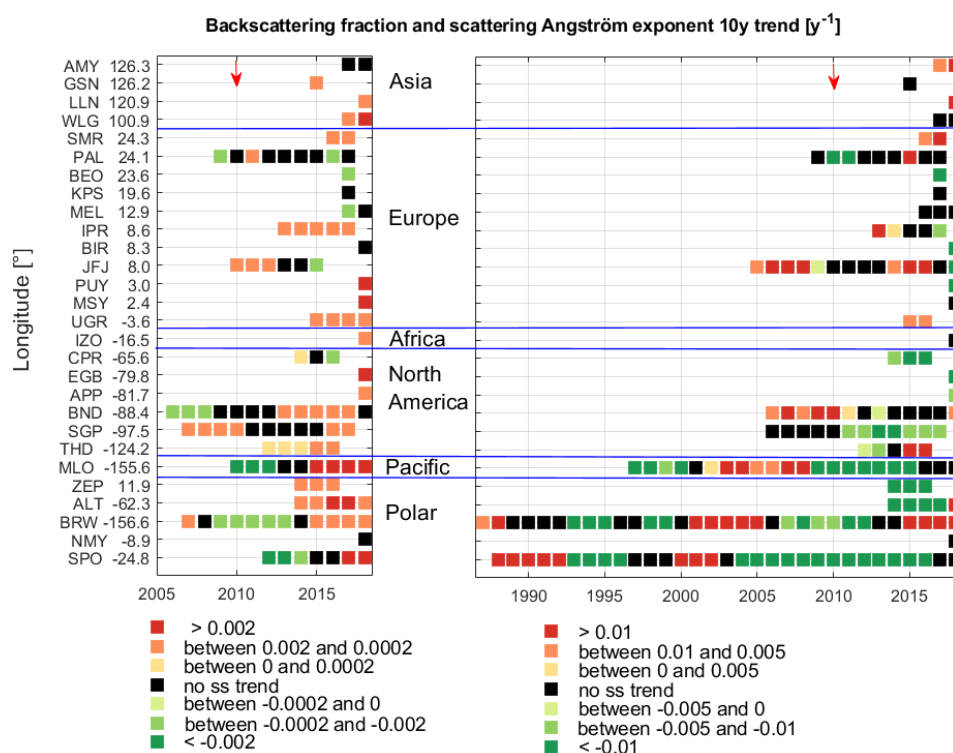
Figure 15: Time series of sequential 10 y b and å$_{sp}$ trends as a function of station longitude. The red arrows indicate the end of the time period covered in CC2013.
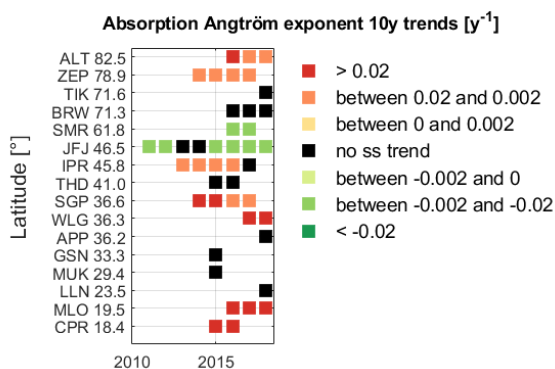
Figure 16: Time series of sequential 10 y å$_{ap}$ trends as a function of station latitude.
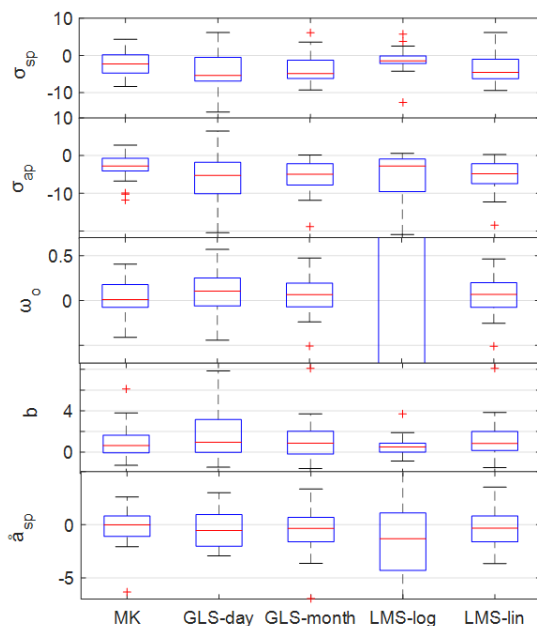
Figure 17: Median, interquartile ranges and whiskers of the slopes in %/y computed by the five methods for the scattering coefficient, the absorption coefficient, the single scattering albedo, the backscattering fraction and the scattering Angström exponent. The outliers are not always visible in the figure for the purpose of clarity.
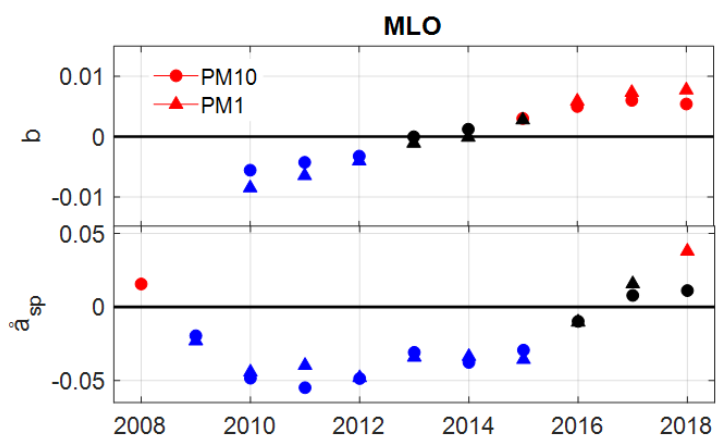
Fig 18: 10 y slopes of b and $\mathring{a}_{sp}$ at MLO. Ss negative and positive trends are plotted in blue and red, respectively. Not ss trends are plotted in black. The dots correspond to PM10 and the upwards triangles to PM1.